Author's personal copy

Provided for non-commercial research and educational use only.
Not for reproduction, distribution or commercial use.

This chapter was originally published in the book *Hydropedology*. The copy attached is provided by Elsevier for the author's benefit and for the benefit of the author's institution, for non-commercial research, and educational use. This includes without limitation use in instruction at your institution, distribution to specific colleagues, and providing a copy to your institution's administrator.

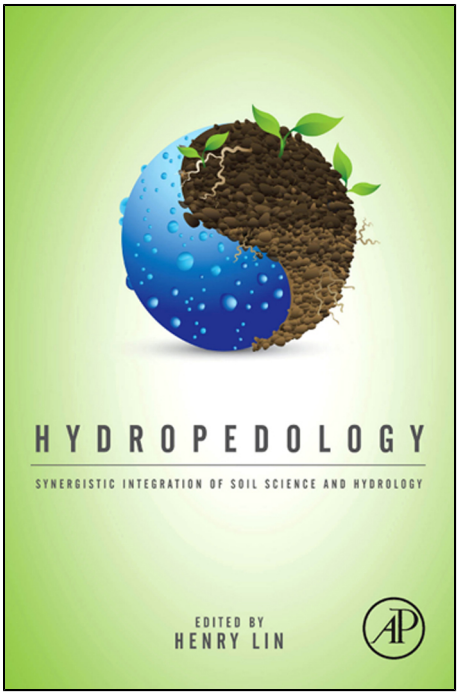

All other uses, reproduction and distribution, including without limitation commercial reprints, selling or licensing copies or access, or posting on open internet sites, your personal or institution's website or repository, are prohibited. For exceptions, permission may be sought for such use through Elsevier's permissions site at:
http://www.elsevier.com/locate/permissionusematerial

From Heimsath, A.M., 2012. Quantifying Processes Governing Soil-Mantled Hillslope Evolution. In: Lin, H. (Ed.), Hydropedology: Synergistic Integration of Soil Science and Hydrology. Academic Press, Elsevier B.V., pp. 205–242.
ISBN: 9780123869418
Copyright © 2012 Elsevier B.V. All rights reserved.
Academic Press

Author's personal copy

Chapter 7

Quantifying Processes Governing Soil-Mantled Hillslope Evolution

Arjun M. Heimsath[1]

ABSTRACT

This chapter presents an overview of how field-based methods quantify the processes shaping upland, soil-mantled landscapes. These methods have been applied across diverse field areas, ranging from the tropical sandstones of northern Australia to the alpine granites of the Sierra Nevada in California. In all cases, the landscapes examined through such work are relatively gently sloping with a generally continuous soil mantle. Soil on such upland landscapes is distinctly defined to be the physically mobile layer derived primarily from the underlying parent material with organic content from native flora and fauna. These upland soils are distinguished from agriculture or lowland soils by the convex-up, hilly topographies that are the focus of this study. Parent material is generally saprolite, i.e. weathered bedrock that retains relict rock structure and is physically immobile. Processes shaping such landscapes include the physical and chemical processes that weather the parent material, and the processes moving the soil downslope. These processes are quantified using several different field-based methods. In situ produced cosmogenic nuclides (^{10}Be and ^{26}Al) are measured in the parent material directly beneath the mobile soil mantle and define the relationship between soil production rates and the overlying soil thickness. The same cosmogenic nuclides are measured in detrital sediments sampled from local channels to quantify basin-averaged erosion rates. Mobile and trace elements are measured in both the parent material and the soils to define chemical weathering rates and processes. Short-lived, fallout-derived isotopes (^{210}Pb, ^{137}Cs, and ^{7}Be) are measured in soil profiles to quantify sediment-transport processes and short-term erosion rates. Parent material strength (competence), or resistance to shear, is measured using a hand-held shear vane as well as a cone penetrometer. The methodology for some results and the connections drawn from this diverse toolbox are summarized in this chapter. An important conclusion connecting parent material strength to the physical processes transporting soil and the chemical processes weathering the parent material emerges with the observation that parent material strength increases with overlying soil thickness and, therefore, the weathered extent of the saprolite. This observation highlights the importance of quantifying

[1]School of Earth and Space Exploration, Arizona State University, AZ, USA.
Email: Arjun.Heimsath@ASU.edu

Hydropedology, Edited by H. Lin. DOI: 10.1016/B978-0-12-386941-8.00007-1
Copyright © 2012 Elsevier B.V. All rights reserved.

Author's personal copy

hillslope hydrologic processes at the same locations where the measurements described herein are made. Specifically, by understanding the hydrologic pathways that help drive the weathering processes of upland soils and saprolites, we will gain considerably greater insight into how the processes described in this chapter drive landscape evolution.

1. INTRODUCTION

Quantifying the rates of Earth surface processes across soil-mantled landscapes is critical for many disciplines (Anderson, 1994; Bierman, 2004; Dietrich et al., 2003; Dietrich and Perron, 2006). Balances between soil production and transport determine whether soil exists on any given landscape, as well as how thick it might be. Soil presence and thickness, in turn, help support much of the life that we humans are familiar with, play important roles in the hydrologic cycle, and are coupled with processes that impact the atmosphere. Similarly, sustainability of the Earth's soil resource under growing human population pressures also depends on the balance between soil production and erosion: agriculture depends on soil. Fully quantifying the conditions that will lead to a depletion of the soil resource is as important, in my opinion, as quantifying the degradation of our drinking water. As such, the near-surface environment that includes soil and its parent material is known as the Critical Zone (CZ) and is the focus of exciting new research initiatives, including the NSF-supported Critical Zone Observatory program (Amundson et al., 2007; Anderson et al., 2004; Anderson et al., 2007; Brantley et al., 2007). Over the last ten years, significant progress in the field (e.g. Anderson and Dietrich, 2001; Burkins et al., 1999; White et al., 1996; Yoo et al., 2007), lab (e.g. White and Brantley, 2003), and with modeling (e.g. Minasny and McBratney, 2001; Mudd and Furbish, 2006) has enabled a new level in understanding how forces of sediment production and transport shape landscapes and help determine the viability of the Earth's soil resource (Montgomery, 2007). Despite this progress, there are significant gaps in our understanding of this interface between humans, the atmosphere, biosphere, and lithosphere. One of the most significant gaps is quantifying what controls soil thickness (Anderson et al., 2007; Brantley et al., 2007), while another is the continued quantification of the sediment-transport relationships (*cf* Geomorphic Transport Laws, Dietrich et al., 2003; Heimsath et al., 2005). The focus of this chapter is on soil-mantled, upland landscapes to provide an overview of how we quantify the rates and processes active in shaping such landscapes. This chapter is not a comprehensive review of the field, but does serve well to review some of the key methods and results applied on these landscapes.

Hilly and mountainous landscapes around the world are mantled with soil. In regions where external sources of sediment (e.g. eolian and glacial deposition) are absent or negligible, the soil mantle is typically produced from the underlying bedrock. Gilbert (1877) first suggested that the rate of

Author's personal copy

soil production from the underlying bedrock is a function of the depth of the soil mantle. We term this rate law the soil production function (Heimsath et al., 1997) – defined as the relationship between the rate of bedrock conversion to soil and the overlying soil thickness. This soil depth that sets the rate of soil production is a result of the balance between the soil production and erosion. If local soil depth is constant over time, the soil production rate equals the erosion rate, which equals the lowering rate of the land surface. Quantifying the soil production function therefore furthers our understanding of the evolution rates of soil-mantled landscapes (Anderson and Humphrey, 1989; Rosenbloom and Anderson, 1994; Dietrich et al., 1995; Heimsath et al., 1997). Heimsath et al. (1997, 1999, 2000) reported spatial variation of erosion rates, suggesting that the landscapes were out of the state of dynamic equilibrium, as first conceptualized by Gilbert (1877, 1909) and then Hack (1960). Such a condition, where the landscape morphology is time-independent, was an important assumption for landscape evolution models. Showing that upland landscapes are actually evolving with time helped spur a new level of understanding for how landscapes change under climatic and tectonic forcing.

On actively eroding hilly landscapes, characterized by ridge and valley topography (Fig. 1), the colluvial soil mantle is typically thin and is produced and transported by mechanical processes. Tree throw, animal burrowing, and similar processes, such as freeze–thaw and shrink–swell cycles, convert in-place bedrock to a mobile, often rocky, soil layer that is then transported downslope by the same actions (Lutz and Griswold, 1939; Lutz, 1940; Lutz, 1960; Hole, 1981; Mitchell, 1988; Matsuoka, 1990; Schaetzl and Follmer, 1990; Norman et al., 1995; Paton et al., 1995). On steep slopes, shallow landsliding also transports

FIGURE 1 Photograph of a typical hilly, soil-mantled landscape that is the focus of work described in this chapter. Point Reyes, California. *(Photo by the author) (Color version online)*

Author's personal copy

material downslope, and may also play a role in producing soil. While such processes are aided directly, and even accelerated, by chemical weathering of the bedrock, they are able to produce soil from bedrock irrespective of its weathered state. Early quantification of the soil production function focused on low-gradient topography developed on relatively homogeneous bedrock, where simple rate laws can characterize the geomorphic processes (Heimsath et al., 1997, 1999, 2000, 2009). Methods applied in those studies were also applied to steep, landslide-dominated landscapes to extend our understanding of the connections between soil production, erosion, and landscape evolution (Heimsath et al., 2001a; Heimsath et al., 2012).

In this chapter, I review the conceptual framework used to quantify soil production and hillslope weathering rates, and explore the field measurements that we make to connect processes governing hillslope hydrology with soil production and transport. Specifically, I will review the mass-balance approach used to model landscape evolution and identify the key field-based parameters that we quantify with direct measurements. These measurements include (1) cosmogenic nuclides (^{10}Be and ^{26}Al) to quantify soil production and catchment-averaged erosion rates, (2) major and trace element analyses to quantify the weathered state and weathering rate of the parent material and soil, (3) short-lived isotopes (^{137}Cs and ^{210}Pb) and optically stimulated luminescence (OSL) to quantify soil transport processes, and (4) cone penetrometer and shear vane measurements to quantify the competence of the parent material underlying the actively eroding soil mantle (i.e. its resistance to physical disruption). This chapter is deliberately focused on expanding upon the methods that we use to examine hilly and mountainous landscapes that are continuously mantled with soil, which is actively produced from the underlying parent material. Instead of focusing on any specific field site, which our various papers do, I will present representative results in a more general way to enable the discussion that will conclude this chapter. To help provide context for these results drawn from different landscapes and studies, I provide a brief overview of how they are all related following the summary of the conceptual framework and methods.

2. CONCEPTUAL FRAMEWORK AND METHODS

2.1. Soil Production and Chemical Weathering

Consider a depth profile at a hillcrest, extending from the soil surface to unweathered bedrock (Fig. 2). The layer of physically and/or chemically altered material (saprolite and soil) atop crystalline bedrock can be millimeters to tens of meters thick depending on the landscape in question and the external driving forces eroding the landscape. A number of definitions are found throughout the literature for these terms; here, 'soil' is the physically mobile material that is produced by the mechanical disruption of the underlying

Author's personal copy

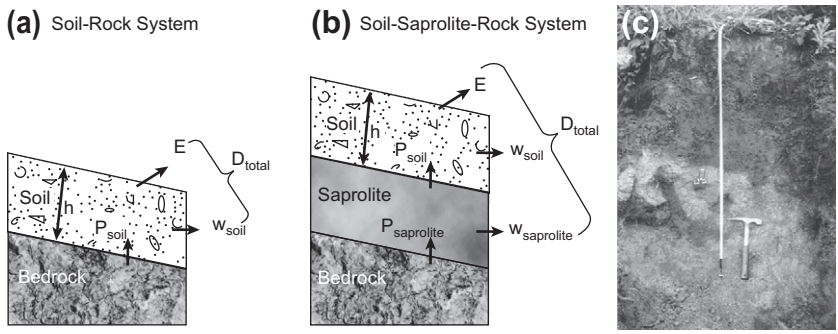

FIGURE 2 Conceptual cross section of soil–saprolite–bedrock showing fluxes and symbols. Soils may be mechanically produced from bedrock (a) or weathered saprolite (b). Based on conservation of mass Eqns (1) and (2) in text, if soils have a steady-state thickness, then soil production (P_{soil}) is balanced by weathering (W_{soil}) and erosion (E). If saprolite thickness attains a similar steady state, then saprolite production (P_{sap}) is balanced by mass loss from the saprolite profile by weathering (W_{sap}) and the mechanical conversion to soil (P_{soil}). Note that total denudation rate (D_{total}) is calculated from the sum of losses, and reflects only erosion and weathering in soil in Fig. 1a, but accounts for the additional losses due to saprolite weathering in Fig. 1b. (c) Photograph of a typical soil-weathered bedrock boundary with gopher burrow shown penetrating the light-colored saprolite. *(From Dixon et al., 2009a)*

bedrock (Fig. 2b), or saprolite (Fig. 2c). Saprolite is the nonmobile, weathered mantle produced by chemical alteration of the bedrock that lies beneath. At the upper boundary, saprolite is incorporated into the mobile soil column through physical disruption by soil production mechanisms such as tree throw, macro- and microfauna burrowing, and frost cracking. At the lower boundary, saprolite is produced from parent bedrock by chemical dissolution and mineral transformation. While mineralogical changes and alteration occur throughout the saprolite column, much of the chemical mass loss can occur as a discrete weathering front near the bedrock boundary (Frazier and Graham, 2000; Buss et al., 2004; Fletcher et al., 2006; Lebedeva et al., 2007; Buss et al., 2008). We focus specifically on the mass loss due to chemical processes (here termed chemical weathering) and physical processes (here termed erosion) on soil-mantled hillslopes. By these definitions, weathering within saprolite is purely chemical, while soils evolve by both chemical transformations and physical disruption and erosion.

Using basic mass conservation principals, any change in soil mass, expressed as the product of soil density (ρ_{soil}) and change in soil thickness (h), reflects the mass rates (determined with the appropriate bulk density measurements times the rate) of soil production (P_{soil}), erosion (E), and weathering (W_{soil}), such that

$$\rho_{soil} \frac{\partial h}{\partial t} = P_{soil} - E - W_{soil}. \quad (1)$$

Author's personal copy

If soil thickness (h) is constant over time $\left(\frac{\partial h}{\partial t} = 0\right)$, then the rate of soil mass loss equals the rate of soil production:

$$P_{\text{soil}} = E + W_{\text{soil}}. \tag{2}$$

The sum of all rates of mass loss can be termed the total denudation rate (D_T), and these losses occur by physical erosion of soil and chemical weathering in both the soil (W_{soil}) and the saprolite (W_{sap}), such that (Fig. 2c)

$$D_T = E + W_{\text{total}} = E + W_{\text{soil}} + W_{\text{sap}}. \tag{3}$$

Recalling mass conservation for steady-state soil thickness Eqn (2), and Eqn (3) can be written as

$$D_T = P_{\text{soil}} + W_{\text{sap}}. \tag{4}$$

It is important to note from Eqn (4) that the soil production rate (P_{soil}) is smaller than the total denudation rate (D_T) in a landscape that experiences chemical weathering in the saprolite. Furthermore, P_{soil}, which can represent a rate of mass flux, can be converted to a landscape lowering rate in units of length per time by dividing by saprolite density if the analyses are done in mass loss per time. D_T cannot as easily be converted into a lowering rate because of its associated saprolite weathering term in Eqn (4); saprolite weathering is observed to be isovolumetric for the studies examined through this conceptual framework, and mass is lost from the saprolite without a corresponding change in volume.

Rates of chemical weathering in catchments have commonly been quantified using stream solute data. These measurements provide a valuable quantification of instantaneous weathering, but provide limited insight into landscape evolution due to their short measurement timescales (1–10 y) and because they integrate mass losses from all points within the catchment, thus treating a watershed as a black box. Riebe et al. (2003a) developed a method to calculate chemical weathering rates in actively eroding terrains by coupling a mass-balance approach using immobile elements (Brimhall et al., 1992; Brimhall and Dietrich, 1987) to rates of landscape lowering derived from cosmogenic radionuclides (CRNs). CRNs such as ^{10}Be and ^{26}Al provided a tool to measure surface rates of denudation over longer timescales (10^3–10^5 y) than solute measurements (1–10 y). These longer timescales, though still only a fraction of the evolutionary period of some landscapes, are more relevant to studies examining the influence of external forcing (climate and tectonics) on landscape change.

CRN concentrations in a sample of rock, saprolite, or soil record the rate of surface denudation processes that removed overlying mass, and

Author's personal copy

therefore the rate at which the sample approaches the land surface (Lal, 1991):

$$D_{\mathrm{CRN}} = \frac{P_0 \Lambda}{N}. \tag{5}$$

Here, the CRN-derived surface denudation rate ($D_{\mathrm{CRN;}}$ g cm^{-2} y^{-1}) is a function of the measured CRN concentration in quartz (atoms g^{-1}), the CRN production rate at the surface (P_0: atoms g^{-1} y^{-1}), which decreases exponentially with depth, and the CRN attenuation length (Λ; g cm^{-2}). A complete version of Eqn (5), used to calculate rates in this chapter, is presented and discussed thoroughly by Balco et al. (2008); however, the simplified version shown by Eqn (5) is sufficient for the purposes of our discussion. For ^{10}Be, the most widely used CRN for determining landscape denudation rates, the penetration depths of cosmic rays, assuming a mean attenuation of 160 cm^2 kg^{-1}, are ~140 cm through soil and ~60 cm through rock (Balco et al., 2008). Nuclide concentrations, therefore, record near-surface mass removal within the top few meters of the Earth's surface, and therefore will reflect both chemical and physical losses within soil (typically less than 2 m thick); however, mass losses due to chemical weathering at the bedrock–saprolite boundary are likely to occur at deeper depths than recorded by CRNs. These losses remain unknown and highlight an outstanding research area for future work. A sample of soil, saprolite, or rock will, therefore, have a ^{10}Be concentration that reflects the rate at which overlying soil was removed. Assuming local steady-state soil thickness (Eqn (2)), this rate is equivalent to the soil production rate (Heimsath et al., 1997, 1999; Heimsath, 2006):

$$D_{\mathrm{CRN}} = P_{\mathrm{soil}}. \tag{6}$$

Here, we caution that the generic term denudation (D_T) should not be used to specifically denote CRN-derived rates of landscape lowering. CRN-derived rates do not capture the result of deep saprolite weathering, and thus only record a portion of total denudation on deeply weathered landscapes. As a consequence, we distinguish between soil production rates (P_{soil}) that equal CRN-derived surface denudation rates (D_{CRN}) and total denudation rates (D_T) that reflect combined rates of mass loss in soil and saprolite due to physical and chemical processes. To fully quantify the potential mass loss from deep saprolite chemical weathering, we expand upon previously developed methods for determining soil production, erosion, and chemical weathering rates.

The enrichment of an immobile element in a weathered product relative to the parent material can be used to calculate the fraction of mass that was lost to chemical weathering (Brimhall et al., 1992; Brimhall and

Author's personal copy

Dietrich, 1987). Riebe et al. (2001b) termed this relationship the chemical depletion fraction (CDF):

$$\mathrm{CDF} = \left(1 - \frac{[I]_p}{[I]_w}\right), \tag{7}$$

where the subscripts 'p' and 'w' refer to concentrations of the immobile element (I) in the parent material and weathered material, respectively. For accurate calculation of the CDF, several important conditions must be met: homogeneous parent material, chemical immobility of the reference element, and minimal chemical weathering during lateral soil transport, which is also an area of active research. Additionally, we must assume no inputs of the immobile element by volcanic ash or continental dust, although this highlights the need for further studies to fully constrain such potential inputs.

Equation (7) can be used to represent the chemical depletion fraction due to soil weathering, saprolite weathering, or total weathering processes. We term these respective depletion fractions the $\mathrm{CDF_{soil}}$, $\mathrm{CDF_{sap}}$, and $\mathrm{CDF_{total}}$, and each is written as Eqn (7), replacing the generic immobile element 'I', with the element zirconium, which is immobile in most weathering environments (e.g. Green et al., 2006).

Following Riebe et al. (2003a), the total chemical weathering rate is the product of the total denudation rate and the total CDF:

$$W_{\mathrm{total}} = D_T \times \left(1 - \frac{[\mathrm{Zr}]_{\mathrm{rock}}}{[\mathrm{Zr}]_{\mathrm{soil}}}\right) = D_T \times \mathrm{CDF_{total}}. \tag{8}$$

Here, the $\mathrm{CDF_{total}}$ represents the fraction of total denudation (D_T) that occurs by all chemical losses (in both the saprolite and the soil). Assuming steady-state soil and saprolite thickness, the saprolite weathering rate can be similarly written (Dixon et al., 2009a). The soil weathering rate is then the calculated difference between W_{total} and W_{sap}.

Calculations of chemical weathering and erosion rates require the measurement of CRN-derived soil production rates. Taking this into account, we rearrange the equations for erosion and weathering in terms of CRN-derived P_{soil} (Eqn (5)). The weathering rate of soil (W_{soil}) is calculated as the product of P_{soil} and the $\mathrm{CDF_{soil}}$:

$$W_{\mathrm{soil}} = D_T \times \left(1 - \frac{[\mathrm{Zr}]_{\mathrm{saprolite}}}{[\mathrm{Zr}]_{\mathrm{soil}}}\right) = P_{\mathrm{soil}} \times \mathrm{CDF_{soil}}. \tag{9}$$

Here, the $\mathrm{CDF_{soil}}$ represents the fraction of original saprolite mass lost due to chemical weathering. The erosion rate (E) can then be calculated as the difference between P_{soil} and W_{soil} (following Eqn (2)).

Lastly, the rate of saprolite weathering (W_{sap}) is calculated by returning to basic principles regarding conservation of mass for immobile elements. For

Author's personal copy

a chemically immobile element such as Zr, the conservation of mass equation can be written as

$$P_{\text{sap}} \times [\text{Zr}]_{\text{rock}} = P_{\text{soil}} \times [\text{Zr}]_{\text{saprolite}} = E \times [\text{Zr}]_{\text{soil}}. \quad (10)$$

Here, P_{sap} (Fig. 2b) represents the rate conversion of rock to saprolite, and is mathematically equivalent to the total denudation rate (D_T) assuming a steady-state regolith thickness. Solving for total denudation yields

$$D_T = P_{\text{sap}} = P_{\text{soil}} \left(\frac{[\text{Zr}]_{\text{saprolite}}}{[\text{Zr}]_{\text{rock}}} \right). \quad (11)$$

Substituting Eqn (11) into a form of Eqn (8) for saprolite then gives us the equation for the saprolite weathering rate (W_{sap}):

$$W_{\text{sap}} = P_{\text{soil}} \times \left(\frac{[\text{Zr}]_{\text{saprolite}}}{[\text{Zr}]_{\text{rock}}} - 1 \right). \quad (12)$$

Summing calculated weathering and erosion rates from these equations allows one to calculate the total denudation rates (Eqn (3)) (Dixon et al., 2009a). These equations differ from those of Riebe et al. (2003a) by the definition that CRN-derived rates reflect only soil production rates, and not total denudation rates in regions mantled by saprolite.

2.2. Soil Transport

The conceptual framework used for our studies is based on the equation of mass conservation for physically mobile soil overlying its parent material (Carson and Kirkby, 1972; Dietrich et al., 1995). Typically, the boundary between soil and the underlying weathered (or fresh) bedrock is abrupt and can be defined within a few centimeters. Soil is produced and transported by mechanical processes, and soil production rates decline exponentially with depth (Heimsath et al., 1997, 2000). The transition from soil-mantled to bedrock-dominated landscapes occurs when transport rates are greater than production rates (Anderson and Humphrey, 1989) and two transport functions are typically used to model landscape evolution (Braun et al., 2001; Dietrich et al., 2003). The slope-dependent transport law has its basis in the characteristic form of convex, soil-mantled landscapes assumed to be in equilibrium, and has some field support (e.g. McKean et al., 1993; Roering et al., 2002). A nonlinear, slope-dependent transport law also has its roots in morphometric observations, and has recent support with the veracity of assuming landscape equilibrium (Roering et al., 1999), experimental constraints (Roering et al., 2001), or for landscapes where postfire ravel processes are thought to dominate (Gabet et al., 2003; Roering and Gerber, 2005; Lamb et al., 2011).

Author's personal copy

Mechanistically, soil transport should depend on soil thickness as well as slope, as suggested by quantification of freeze–thaw (e.g. Anderson, 2002; Matsuoka and Moriwaki, 1992), shrink–swell (e.g. Fleming and Johnson, 1975), viscous or plastic flow (e.g. Ahnert, 1976), and bioturbation processes (Gabet, 2000). In each case, disturbance processes set the mobile soil thickness and modulate soil transport by setting the magnitude of slope-normal displacement, while slope sets the downslope component of the gravitational driving force. Depth-dependent flux is also suggested by the velocity profiles from segmented rod studies and modeling (Young, 1960; Young, 1963). For flux to be proportional to the depth–slope product is an idea that has never been tested despite being suggested almost 40 years ago (Ahnert, 1967).

Recently, Furbish (2003) suggested that for transport due to dilational effects of biotic activity, the vertically averaged volumetric flux density (i.e. vertically averaged velocity), $\overline{q}_s$ (L t^{-1}), is proportional to land surface gradient, S. The depth-integrated flux per unit contour distance is then the product of soil thickness, H, and this flux density

$$H\overline{q}_s = -K_h H S, \tag{13}$$

where K_h (L t^{-1}) is a transport coefficient, assumed to be constant. We tested this transport relation using estimates of local depth-integrated flux, $H\overline{q}_s$, obtained by integrating the soil production rate between flow lines at three distinct field sites (Heimsath et al., 2005), and found support for the depth-dependent transport relationship (Furbish et al., 2009). Importantly, our work quantifying the soil production function using both CRNs and the morphometric test of plotting topographic curvature against soil thickness also supports the slope-dependent transport relationship (Heimsath et al., 1997, 1999, 2000, 2006). Clearly, more direct quantification of the soil transport processes is needed and some of our studies are pursuing this actively.

Long-standing efforts to determine average erosion rates across agricultural landscapes involve the construction of small-scale runoff plots (Roels, 1985), monitoring of suspended sediment concentrations in streams draining the landscapes (Steegen et al., 2001), and, with recent analytical breakthroughs, through the use of sediment tracers (Matisoff et al., 2001) or short-lived isotopes (Wilson et al., 2003; Matisoff et al., 2002a,b). Collection and analyses of soil from runoff plots or suspended sediment analyses remain problematic primarily because of the difficulties with ensuring a closed system, while injection of tracers onto agricultural lands immediately imparts a short-term measurement bias. Attempts to quantify sediment-transport processes include segmented rod studies (Young, 1960), tephra deposit mapping (Roering et al., 2002), detailed measurement of bioturbation (Black and Montgomery, 1991; Gabet, 2000), optically stimulated luminescence dating of individual quartz grains (Heimsath et al., 2002), and short-lived isotope measurements (Wallbrink and Murray, 1996; Walling and He, 1999; Kaste et al., 2007; Dixon et al., 2009a). Despite the

Author's personal copy

extensive effort across disciplines, quantifying sediment-transport processes and rates remains elusive (Dietrich et al., 2003).

During the middle of the twentieth century, the detonation of nuclear weapons in the atmosphere injected a host of artificial radionuclides into the environment with half-lives ranging from days to decades. While atmospheric weapons were tested in various countries from the 1940s until the late 1970s, the vast majority of fallout in the central United States was deposited between 1955 and 1967 (Cambray et al., 1989; Simon et al., 2004). These fallout radionuclides offer a unique tool for determining time-integrated erosion rates on a landscape with only one or a few visits to the site (Brown et al., 1981a; Brown et al., 1981b; Zhang et al., 1994; Quine et al., 1997; Walling et al., 1999; Walling et al., 2002; He and Walling, 2003; Porto et al., 2003; Fornes et al., 2005). Fallout radionuclides are used extensively in erosion and sediment-transport studies on both agricultural and forested landscapes. Atmospherically delivered ^{210}Pb ($T_{1/2} = 22.3$ y, $^{210}Pb_{ex}$, "in excess" of that supported by direct decay of ^{222}Rn in soil), cosmogenic ^{7}Be ($T_{1/2} = 53$ d), and weapons-derived ^{137}Cs ($T_{1/2} = 30.1$ y) and ^{241}Am ($T_{1/2} = 432$ y) can be used alone or simultaneously to quantify and trace erosional processes (Wallbrink and Murray, 1996; Walling et al., 1999; Whiting et al., 2001), date and source sediments (Appleby and Oldfield, 1992), and determine sediment transit times (Bonniwell et al., 1999). Fallout radionuclides are useful geomorphic tools because of their unique atmospheric source term, but the technique relies on the assumption that the radionuclides are geochemically immobile and thus effective particle tracers.

Relative rates of soil mixing can be evaluated through measurements of fallout nuclide activities in soil profiles (Dörr, 1995; Tyler et al., 2001). Because these atoms are deposited at the soil surface, mixing processes can increase the dispersion of nuclides with depth and the overall downward transport rate. For example, on agricultural landscapes, where tilling homogenizes the soil to the depth of the plow layer, a unique, well-mixed ^{137}Cs profile captures the process (Walling et al., 1999). Field evidence suggests that some soils are homogenized naturally by burrowing organisms (Heimsath et al. 2002; Black and Montgomery, 1991), which would mix fallout isotopes down to a depth governed by the flora and fauna at the site. However, in some undisturbed forest soils where bioturbation is less obvious, the transport mechanisms can be more elusive and difficult to quantify. By measuring the vertical distribution of fallout radionuclides in soils and calculating diffusion coefficients, we can quantify sediment-transport mechanisms and mixing rates that are operating on the short but important timescale of 10–100 years.

The techniques of relating fallout radionuclide profiles and inventories to absolute and relative erosion rates rely on finding a "noneroding" reference location to compare to eroding or aggrading sites (Lowrance et al., 1988). Nearly all erosion studies by other research groups compare soils sampled at cultivated sites with those sampled from an undisturbed field or forest. We examined soil mixing and transport processes across our soil-mantled

Author's personal copy

hillslopes using fallout radionuclides and by observations of biological activity in the field. We measured $^{210}Pb_{excess}$ (here, shortened to ^{210}Pb) and ^{137}Cs nuclide activities with depth and calculated total inventories, to gain insight into mixing (e.g. Kaste et al., 2007; Dixon et al., 2009a) and soil erosion mechanisms (e.g. Kaste et al., 2006; O'Farrell et al., 2007). The nuclide profile depth was defined as the soil depth at which greater than 95% of the cumulative nuclide activity, or inventory, was obtained. We used nuclide profiles to determine the degree of physical mixing, and calculated a mixing coefficient by the best-fit exponential curve to an advection–diffusion equation (Kaste et al., 2007).

Steady-state profiles of ^{210}Pb provide insight into mixing and soil transport over short timescales (10^2–10^3 years). The depth distribution of ^{210}Pb in soils can be described by the steady-state solution to the advection–diffusion equation (e.g. He and Walling, 1996; Kaste et al., 2007):

$$A(z) = A_0 \exp\left[\frac{v - \sqrt{v^2 + 4\lambda D}}{2D}(z)\right], \tag{14}$$

where '$A(z)$' is the nuclide activity at a specific depth (in Bq cm^{-3}), 'A_0' is the activity at the surface, 'v' is the downward advection velocity due to leaching (cm y^{-1}), 'λ' is radioactive decay (y^{-1}), and 'D' is a diffusion-like mixing coefficient (cm^2 y^{-1}). Advection rates have previously been measured using the depth of concentration of weapons-derived ^{137}Cs, which was delivered to soils as a thermonuclear bomb product between 1950 and 1970, peaking in 1964 (e.g. Kaste et al., 2007). We were sometimes unable to determine clear subsurface peaks in ^{137}Cs activity profiles that correspond to this delivery. Instead, in such cases, we calculated diffusion-like mixing coefficients by assuming that advection plays a minimal role in subsurface nuclide redistribution. We then modeled a best-fit diffusion equation to each profile by minimizing the sum of residuals. Importantly, the timescale of such quantification is only appropriate for recently (~10 to <100 years) active processes.

2.3. Parent Material Strength

The depth dependency of soil production rates followed Gilbert's early reasoning that rock disintegration was fastest under thin soils and slowed where bedrock emerged at the surface or was deeply mantled with soil. Gilbert believed that on a steady-state landscape, where erosion is equaled by soil production, highest erosion rates would be under thin soils and lowest rates would be at the extremes because (i) exposed bedrock would limit transport to the slow rate of exposed and coherent rock and (ii) thick soil cover would develop for low transport rates. While this conceptual framework persisted (Carson and Kirkby, 1972) and was explored extensively (Ahnert, 1967; Anderson and Humphrey, 1989; Cox, 1980; Dietrich et al., 1995; Heimsath

Author's personal copy

et al., 1997; Minasny and McBratney, 1999), the underlying mechanisms governing it remain fundamentally untested. The sharp boundary between saprolite and soil as well as the biogenic disruption by gopher burrowing, ants, earthworms, and burrowing wombats (Australia) are widely observed, highlighting the role of parent material weatherability in setting the upper bound for soil production, as well as biogenic role in downslope transport. Additionally, quantifying parent material strength at locations where soil production and transport rates as well as chemical weathering rates are known helps make the connection between hillslope hydrology and the geomorphic processes driving landscape evolution.

Specifically, the parent material resistance to the physical processes that convert it to transportable sediment is likely to reflect the intersection of several aspects of forces driving landscape evolution. First, tectonic forces set the base level that upland landscape evolution is thought to be responding to. Second, climatic forces set both the biota (i.e. flora and fauna) providing the physical forces of hillslope weathering, and the chemical weathering parameters that break down minerals and remove mass in solution. Third, the combination of physical and chemical weathering processes is likely to determine just how weathered (and therefore resistant to shear) the parent material becomes. For example, active bioturbation that mixes a soil thoroughly also helps convey water and organic acids to the soil-parent material boundary. Conversely, a landscape lacking bioturbation and experiencing active overland flow processes is likely to have a smaller degree of contact between meteoric waters and the parent material. Understanding hillslope hydrologic pathways are, therefore, critically important for coupling the physical and chemical processes that we have focused on thus far. Quantifying all of the different processes and parameters that factor into how hillslopes are evolving thus enables us to better predict how landscapes are likely to change with the changing driving forces of climate, tectonics, and anthropogenic.

We apply independent, field-based measurements to quantify the strength (i.e. resistance to shear) of the parent material underlying the mobile soil layer. Quantifying strength can be done in a number of ways. Selby (1980, 1985) suggests a semiquantitative classification of rock mass strength for crystalline bedrock. Although this method is comprehensive and appropriate for rocky slopes, it is difficult to compare with soil-mantled slopes where we are interested in the saprolite resistance to physical disruption. Several studies have explored the physical characteristics of granitic and metamorphic rocks and saprolites, but have mostly focused on groundwater saturation effects and slope stabilities (e.g. Jiao et al., 2005; Johnson-Maynard et al., 1994; Jones and Graham, 1993; Kew and Gilkes, 2006; Schoeneberger et al., 1995). It is important to note that the complexities inherent in quantifying the strength of competent rocky slopes are lessened by the fact that we are interested in quantifying the resistance of a relatively continuous layer of weathered material that is overlain by a relatively smooth surface mantle of soil.

Author's personal copy

We use two instruments to assess saprolite strength: a dynamic-cone penetrometer and a shear vane tester (Herrick and Jones (2002) and GEONOR). We also experimented with Schmidt hammers (see recent review article and results in Viles et al. (2011)), but their dependence on grain boundaries and limited applicability to competent bedrock meant that we could not use them for saprolitic parent material (i.e. anything experiencing even the slightest degree of weathering). The penetrometer measures the compressibility of a material in units of strikes per depth, which can be converted to kPa when calibrated with the shear vane tester. The shear vane tester measures the shear strength in kilopascals (kPa). We used a Geonor H-60 handheld vane tester (GEONOR) with an instrument range from 0 to 260 kPa. The standard procedure is to place the end of the vane normal to the surface and insert it about 5 cm below the surface to minimize any edge effects, then turn the handle clockwise at a constant rate until the lower and upper portions of the instrument move in unison, indicating that the maximum shear strength has been obtained. Other studies have explored the correlation between these two instruments at different sites (Bachmann et al., 2006; Zimbone et al., 1996). The shear strength of a soil is directly related to the normal stress applied (McKyes, 1989); therefore, an instrument that applies a force normal to the surface can be used to estimate a relative shear strength. Several field seasons of experimenting with these instruments led us to a procedure that appears to yield reproducible and reliable results (Byersdorfer, 2006; Johnson, 2008).

3. FIELD SITE SUMMARY

To tie together the methods outlined above, I draw upon studies across a few selected field areas examined by my research group. It is beyond the scope of this chapter to go into all the details, or expand upon all of the specific assumptions and caveats for each of these study areas, but there are key aspects of the sites that I summarize here to help navigate the connections between the conceptual framework and the representative results. Recall that a key assumption used to develop the conceptual framework is the assumption that soil thickness does not change with time locally. This does not mean that soil thickness is uniform across the landscape, but it does mean that our initial site selection was motivated by convincing ourselves that local soil thickness remains constant (excluding the stochastic perturbations associated with bioturbation that are relatively quickly "healed"). A similarly important criterion for site selection was that the processes we observe today reflect the processes driving landscape evolution over the timescales captured by our methodologies (tens to tens of thousands of years). Three field areas were, therefore, the initial focus of our studies: Tennessee Valley (TV), California, Point Reyes (PR), California, and Nunnock River (NR), southeastern Australia. Each of

Author's personal copy

these field sites has smoothly convex-up soil-mantled ridges separated by unchanneled, "zero-order" swales and also had independent studies, suggesting that the impact of the Pleistocene–Holocene transition on local biota was not severe. Two of these field sites (PR and NR) have granitic parent material, while TV has metasedimentary rock. The relative ease of working on granitic parent material drove further studies to focus on granitic landscapes, where possible.

Following the honing of methodology across these field sites, we expanded our studies to include an examination of the role of climatic forcing. For that work we used a climate transect in the southern Sierra Nevada Mountains (Dixon et al., 2009a,b) and I summarize some of that work here by focusing on the climate end members of the alpine region of Whitebark (WB) and the oak-grassland region at Blasingame (BG). We worked in parallel to examine the role of tectonic forcing by focusing on a series of sites across the San Gabriel Mountains of California (SG) (DiBiase et al., 2010; Heimsath et al., 2012); however, I draw only upon the coupling between parent material strength and soil production for that site here. I do also draw briefly upon work done in a New England Forest (NE) to highlight some differences between processes active on the upland landscapes focused on here and a temperate forest that experienced Pleistocene glaciation. Table 1 summarizes the field sites used to draw the representative results shown here, and does not include other sites that I make only brief note of (e.g. Oregon Coast Range and northern Australia). It also does not list the methods used at or key results from these sites that are not raised in this paper.

4. REPRESENTATIVE RESULTS AND DISCUSSION

4.1. Soil Production

The first quantification of the soil production function was from Tennessee Valley (TV), California, and utilized both ^{10}Be and ^{26}Al measured in the saprolite beneath a range of soil depths (Heimsath et al., 1997, 1999). Further work on both granite and metasedimentary parent material supported the newly developed methodology (Heimsath et al., 2000, 2001a,b) and showed a wide range of application for this transport relationship. More recent work helps illustrate the results well (Heimsath et al., 2005, 2010). Soil production rates from 13 samples from the bedrock–soil interface at Point Reyes (PR) define a clear exponential decline of soil production with soil depth such that the variance-weighted best-fit regression (Fig. 3a) is

$$\varepsilon(H) = (88 \pm 6) \cdot e^{-(0.017 \pm 0.001)H}, \tag{15}$$

where soil production, $\varepsilon(H)$, is in meters per million years and soil depth, H, is in centimeters. Average erosion rates, inferred from three samples of

Author's personal copy

TABLE 1 Summary of Field Sites Reported in this Chapter

Field site (abbreviation)	Methods used	Key results	References
Tenn. Valley (TV)	CRNs, short-lived isotopes	Soil production, depth-dependent transport	Heimsath et al. (1997, 1999, 2005); Kaste et al. (2007)
Point Reyes (PR)	CRNs, chem., strength	Soil production, chem. weathering, parent material strength, depth-dependent transport	Heimsath et al. (2005)
Nunnock River (NR)	CRNs, chem., short-lived isotopes, strength	Soil production, chem. weathering, parent material strength, depth-dependent transport	Heimsath et al. (2000, 2005, 2006, 2010); Kaste et al. (2007)
Blasingame (BG)	CRNs, chem., short-lived isotopes	Soil production, chem. weathering, transport processes	Dixon et al. (2009a,b)
Whitebark (WB)	CRNs, chem., short-lived isotopes	Soil production, chem. weathering, transport processes	Dixon et al. (2009a,b)
New England (NE)	Short-lived isotopes	Lack of soil mixing, short vs. long term *E.*	Kaste et al. (2007)
San Gabriels (SG)	CRNs, strength	Soil production, parent material strength	Heimsath et al. (2012)

stream sand from the creek draining the study area, determine a basin-averaged rate of 62 m/m.y., similar to Tennessee Valley (Fig. 1b). Lower erosion rates from two tors at Point Reyes are consistent with granitic core-stone emergence shown at Nunnock River (NR) (Heimsath et al., 2000). Comparison of the soil production functions reveals remarkable similarity in form with relatively little scatter around the Point Reyes regression line (Fig. 3b). Similar to the Nunnock River and Tennessee Valley sites, these data, combined with the spatial variation of depth data from Fig. 4a, discussed below, show spatially variable rates of soil production, indicating a landscape out of long-term dynamic equilibrium. This is not surprising given the proximity of the San Andreas fault to the site, and the southern California origin of the Point Reyes Peninsula (Heimsath et al., 2005).

Author's personal copy

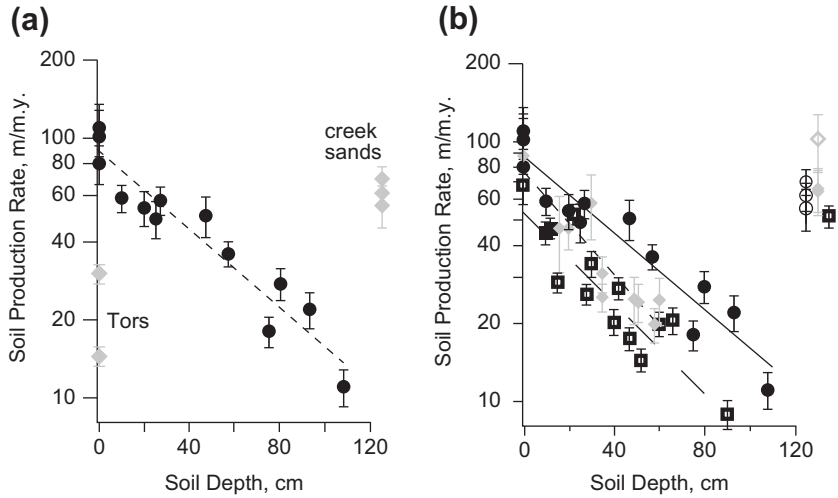

FIGURE 3 Soil production functions. (a) Point Reyes (PR). Solid black circles are averages of rates from both ^{10}Be and ^{26}Al, and error bars represent all errors propagated through nuclide calculations, i.e. uncertainty in atomic absorption, accelerator mass spectrometry, bulk density and soil depth measurements, and attenuation length of cosmic rays. Gray diamonds are erosion rates from outcropping tors on ridge crests. (b) Point Reyes data shown with results from Nunnock River (open black squares, long-dashed regression line, Heimsath et al., 2000) and Tennessee Valley (gray diamonds, short-dashed regression line, Heimsath et al., 1997); open symbols labeled "creek sands" are average rates from detrital cosmogenic nuclide concentrations from each site. *(From Heimsath et al., 2005)*

The Point Reyes results are evidence for the applicability of the soil production function as a transport relationship (cf. Dietrich et al., 2003) characterizing hilly, soil-mantled landscapes. Comparison of functions from these different sites offers the potential for untangling the connections between erosion rates, climate, and tectonics. Specifically, the relationship slope quantifies the depth dependency of the soil-producing mechanisms. Similarity in slope (Fig. 3b) reveals that soil production rates are halved beneath 35 cm of soil and down to a tenth of their respective maxima beneath 115 cm, roughly the maximum soil depth across divergent ridges. Biogenic processes are dominant across each site, are controlled by climate, and potential variations in their effects across the landscapes may be responsible for this order-of-magnitude difference in lowering rates. The absolute magnitude of such disequilibrium is quantified by the slope as well as the intercept of the soil production function, the latter potentially set by the underlying strength, or resistance to erosion, of the parent material. Such disequilibrium would suggest a long-term flattening of noses, a trend that is likely to be offset by the periodic evacuation of the convergent hollows such that local base level to the hillslopes is reset, and ridge–valley topography is maintained (Dietrich et al., 1995) (Pelletier and Rasmussen, 2009).

Author's personal copy

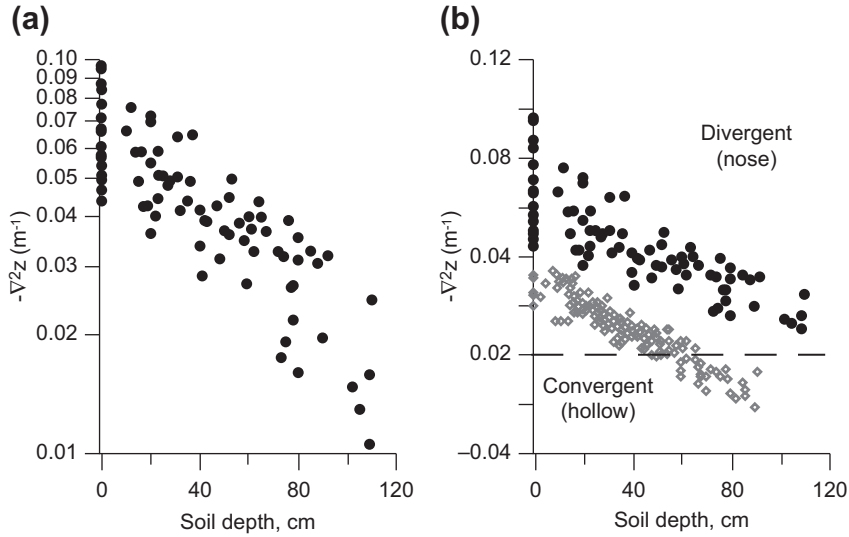

FIGURE 4 Negative curvature versus vertical soil depth. Curvature calculated as in Heimsath et al. (1999) and is proxy for soil production if local soil depth is constant with time. (a) Black circles from individual soil pits at Point Reyes with exponential negative curvature axis. (b) Black circles same as Figure 4a with open gray diamonds from Nunnock River (Heimsath et al., 2000). Tennessee Valley data from Heimsath et al. (1997, 1999) overlay Nunnock River data values and range and are not included here for plot clarity. Black dashed line separates divergent from convergent topography. *(From Heimsath et al., 2005)*

4.2. Chemical Weathering

To connect the soil production function to the chemical weathering processes active across hilly landscapes, we focus on the southern Sierra Nevada Mountains, California (Dixon et al., 2009a,b). We applied our diverse methodology across several field sites ranging from the low elevation oak-grassland landscape at Blasingame (BG) to the alpine region near the crest of the western Sierra at Whitebark (WB). Hillslope soil production rates average 82 ± 10 ton/km^2/a (37 ± 4 m/Ma; mean $\pm$ std error) at the low elevation BG and 52 ± 5 ton/km^2/a (24 ± 2 m/Ma) at high elevation WB site. At BG, soil production rates decrease with increasing soil thickness (Fig. 5a) and distance from the slope crest (Fig. 5b), as observed in other temperate landscapes (e.g. Figs 3a and b). At WB, such a relationship is not observed.

Chemical weathering results in an average net loss of $24 \pm 4\%$ of the soil mass at both sites, calculated as the average CDF_{soil}, and CDF values are not significantly different at the two sites. Dahlgren et al. (1997) observed that clay content of the low elevation soils exceeds that of WB soils by a factor of two. This suggests a discrepancy in how soil weathering intensity is recorded by CDF and clay abundance. The CDF quantifies net elemental losses; however,

Author's personal copy

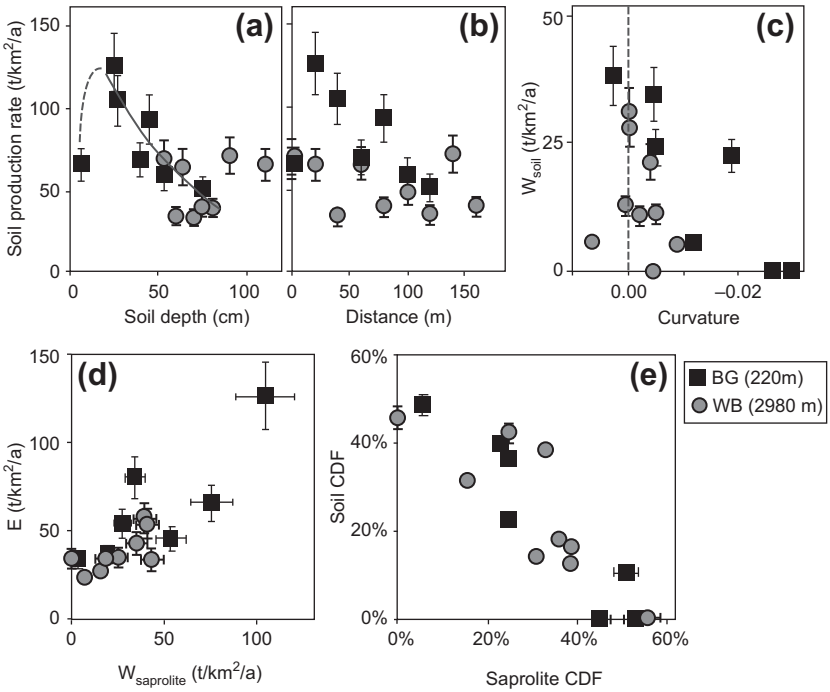

FIGURE 5 Differences in erosion and weathering between high- (Whitebark, WB) and low-elevation (Blasingame, BG) field sites from Dixon et al. (2009b) study. Average ^{10}Be-derived, soil production rates are higher at BG than WB. At BG, these rates decrease with (a) soil thickness and (b) distance from the ridge crest. (c) Soil chemical weathering rates (W_{soil}) decrease with increasing convexity (negative curvature) at BG, and insignificantly at WB. (d) Physical erosion rates (e) increase with the chemical weathering rate of saprolite ($W_{saprolite}$) at both sites. Average rates of erosion are faster at the warmer and drier BG, compared to the colder and wetter WB, although saprolite weathering rates are not significantly different. (E) Soil and saprolite weathering extents, shown by chemical depletion fractions (CDF) are negatively correlated.

secondary mineral formation is the balance between chemical dissolution of primary minerals and the leaching of weathering products. Potential mass loss may exceed net mass loss at low elevation, due to secondary mineral development and retention, in agreement with previous observations of the low leaching potential of clay minerals in these soils compared to high elevation soils (Dahlgren et al., 1997). Thus, the total chemical alteration at BG site is greater despite similar net losses to WB.

At both sites, CDF_{sap} data indicate that saprolite weathering is a large portion of the total weathering losses, averaging $31 \pm 4\%$ and reaching values as high as 56% of the original rock mass. Saprolite weathering rates average 46 ± 13 ton/km^2/a at BG and 25 ± 5 ton/km^2/a at WB. Physical erosion rates at low and high elevations average 64 ± 12 ton/km^2/a and 38 ± 4 ton/km^2/a,

Author's personal copy

respectively. At BG, soil chemical weathering rates decline with increasing convexity (Fig. 5c). Furthermore, physical erosion and saprolite weathering rates at both sites are positively correlated (Fig. 5d), and a strong negative relationship exists between the chemical weathering extents of soils and saprolites (Fig. 5e). In the Discussion section, we explore implications of these data following the quantification of transport processes and the parent material strength.

Chemical weathering facilitates physical erosion by the dissolution of primary minerals, reducing the competency of rock and increasing erodibility. Our data are among the first to quantify links between saprolite weathering and physical erosion. Physical erosion rates increase with saprolite weathering rates (Fig. 5d). These data suggest that physical erosion is dependent on the chemical weathering extent and rate of bedrock, since weathered saprolite is more easily detachable and mobilized into the overlying soil column. Furthermore, soil chemical weathering rates at low elevation decline with increasing convexity (Fig. 2c), and the intensity of chemical weathering in soils and saprolites is inversely related (Fig. 2e). Soil weathering may be low where saprolite weathering is high due to faster erosion that reduces soil residence times (e.g. Anderson, 2002). As water and sediment are shed off divergent areas of the landscape, decreased water–soil interaction could further result in decreased chemical weathering of soils. Conversely, similar CDF_{total} across the Sierras may support the idea that weathering of parent bedrock is limited by the supply of fresh minerals, rather than reaction rates (e.g. Riebe et al., 2000; Riebe et al., 2001a; West et al., 2005). Saprolite weathering in the Sierras, indicated by saprolite CDFs and rates, is controlled by processes not clearly identified from our study, but is possibly linked to climate, moisture availability, and hillslope morphology. Our data suggest that soil weathering is limited by the availability of fresh minerals, and is therefore low when saprolite has previously depleted this supply.

Second, and perhaps most importantly, these data show an example of the strong feedbacks between physical erosion and chemical weathering at both Sierran study sites, despite broad differences between the climates and the soil production and transport mechanisms. Other authors have reported positive correlations between soil chemical weathering and erosion and have suggested that physical erosion sets the pace for chemical weathering (e.g. Riebe et al., 2003b; Riebe et al., 2004) in soil-mantled terrain. Our data indicate saprolite weathering and erosion are positively linked (Fig. 5d), and soil weathering is reduced where both saprolite weathering (Fig. 5e) and landscape convexity (Fig. 5c) are high. In summary, our data suggest that saprolite weathering controls erosion and weathering of the overlying soil by depleting primary minerals, decreasing rock competence, and increasing mobility of weathered material. Since chemical weathering of the saprolite accounts for such significant mass loss from these landscapes, we suggest that not accounting for it leads to missing a critical aspect of erosion–weathering feedbacks.

Author's personal copy

4.3. Soil Transport

Soil depths vary spatially across the divergent areas of the Point Reyes (PR) landscape such that topographic curvature declines exponentially with increasing soil thickness (Fig. 4a), although a linear decline similar to the observations from the Nunnock River (NR) and Tennessee Valley (TV) field sites cannot be ruled out (Fig. 4b). Using curvature as a proxy for soil production (Heimsath et al., 1999), these data support the soil production function defined by Eqn (15), assuming an independently documented (Reneau and Dietrich, 1990, 1991) "linear diffusivity" of 30 $cm^2\ yr^{-1}$. The clear linear (versus exponential) decline of curvature with increasing soil depths at NR suggested, however, that a linear slope-dependent transport model did not adequately capture the transport mechanisms, prompting modeling (Braun et al., 2001) and optically stimulated luminescence (Heimsath et al., 2002) studies highlighting the importance of soil thickness in controlling transport.

We plot depth-integrated flux, determined by integrating soil production rates downslope, against the depth–slope product across all field areas to test the nonlinear transport law of Eqn (13) (Fig. 6a). We observe linear

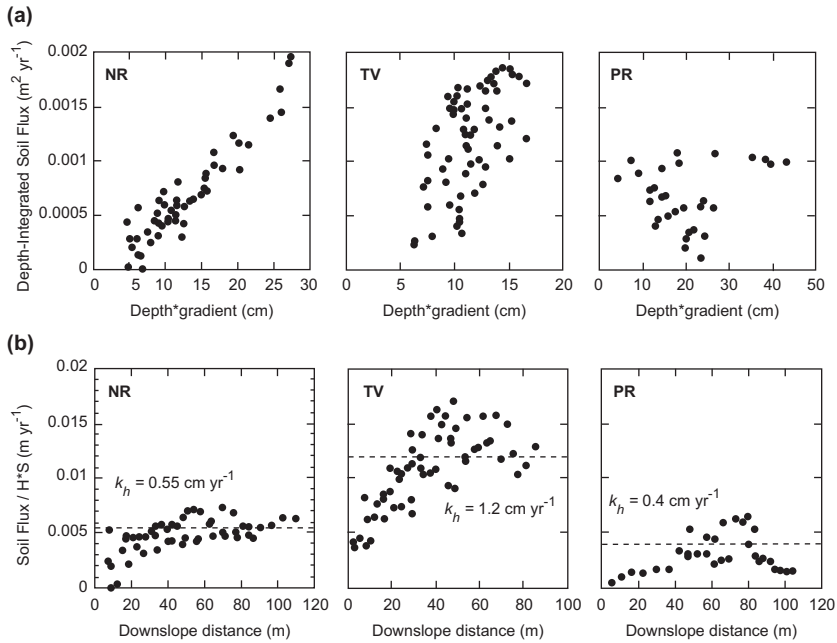

FIGURE 6 (a) Depth-integrated soil flux per unit contour length ($m^2\ yr^{-1}$) versus the depth–slope product (cm) for all field sites as described in Heimsath et al. (2005). (b) Depth-integrated flux divided by depth–slope product versus downslope distance. K_h value, determined by fitting data shown in A, is dashed line. NR, Nunnock River; TV, Tennessee Valley; PR, Point Reyes.

Author's personal copy

increases of soil flux with increasing depth–slope product for both the NR and TV field sites, offering strong support for the depth-dependent transport relationship. Data from NR support Eqn (13) with a transport coefficient, K_h, equal to 0.55 cm yr^{-1}. Roughly equating this coefficient to the linear "diffusivity" with an average soil thickness for Nunnock River of 65 cm yields a coefficient of 36 cm^2 yr^{-1}, which is remarkably similar to the 40 cm^2 yr^{-1} reported by Heimsath et al. (2000). Reversing the process for the TV and PR data, which have independently determined linear "diffusivities" of 50 and 30 cm^2 yr^{-1} and average soil thicknesses of 30 and 50 cm, yields depth-dependent transport coefficients of 1.7 and 0.6 cm yr^{-1}, respectively. Using the data from TV and PR (Fig. 6A), K_h values of 1.2 and 0.4 cm yr^{-1} are determined.

This comparison of transport coefficients places the depth-dependent transport flux within the context of the more familiar slope-dependent transport framework and supports the applicability of a linear transport law for low-gradient, convex landscapes. Plotting flux against gradient shows, however, that a linear relationship does not reflect all the data (Data Repository; see footnote 1). Our test for depth-dependent transport thus involves two sets of complementary plots: $H\overline{q}_s$ versus HS (Fig. 6a) and $H\overline{q}_s(HS)^{-1}$ versus downslope distance, X (Fig. 6b). If Eqn (1) is correct, the first plots (Fig. 6a) should show a linear increase, with slope equal to K_h and zero origin – in the absence of covariance of H or S with distance X. However, because $H\overline{q}_s$ must, by definition, increase with X, these plots might exhibit spurious covariance with the depth–slope product. Thus, the importance of the inset plots (Fig. 6b) is to remove any such covariance such that the data should be homoscedastic about a flat line equal to K_h (dashed line) to support Eqn (1). We observe, instead, an increase with distance close to the ridge crests, followed by a tendency to flatten roughly around the K_h values. Potential explanations for the increase include the unknown role of chemical weathering or a nonconstant, covariant transport coefficient that we have not yet quantified.

Fallout radionuclide activity–depth profiles and field observations reveal distinct differences in sediment-transport processes at the climate end members of our Sierra Nevada field site. Vegetative density is lowest at the high elevation WB, with an average of 83% bare soil versus 4% at BG. Low vegetative cover and high precipitation at WB result in low soil resistance to surface water flow and rain drop splash (e.g. Prosser and Dietrich, 1995). Rills began ~40 m downslope from the crest at WB. These have an upslope spacing of 23 m decreasing to an average spacing of 9 m at ~60 m from the slope crest. No rilling was evident at BG. At both sites, bioturbation is evident in soils, and gopher burrows were observed parallel to the ground surface and as deep as the soil–saprolite interface. Mapping gopher burrow density indicates that the burrowing activity at WB is 53% that of BG (Dixon et al., 2009a).

Author's personal copy

Penetration depths of ^{210}Pb and ^{137}Cs increase linearly with burrowing activity at both sites (Fig. 7a), suggesting that bioturbation – through physical transport and altered hydrology – redistributes nuclides to depth in the soil. Assuming nuclide profiles form primarily by diffusion-like processes, the average diffusive mixing coefficient of soils is 0.28 ± 0.05 cm^2/a at BG, greater than the average 0.15 ± 0.02 cm^2/a at WB (Fig. 7b). ^{210}Pb inventories do not vary consistently with topography at BG; however, at WB, inventories are lowest where slopes are steepest and have the greatest upslope contributing area (Fig. 7c,d). Upslope contributing area has the strongest negative correlation with nuclide inventory at WB, suggesting soil loss scales with

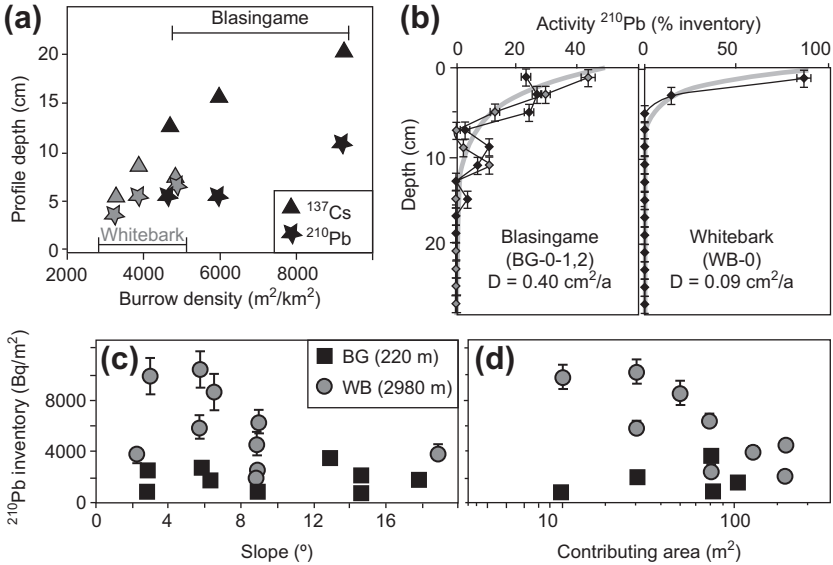

FIGURE 7 (a) Surface-burrowing activities from three transects at BG and WB from Dixon et al. (2009b) increase with associated profile depths for fallout nuclide $^{210}Pb_{excess}$ and ^{137}Cs. "Profile depth" is defined as the soil depth at 95% cumulative nuclide inventory. (b) Fallout profiles show nuclide activity versus depth for hillcrests at BG (two profiles shown are 2 m apart) and WB (one profile) and are deeper at BG. We calculated diffusion-like mixing coefficients for each profile (shown by broad gray line) by the best fit to the diffusion equation, Eqn (14), where '$A(z)$' and 'A_0' are nuclide activity at depth ('z') and surface, respectively, 'λ' is nuclide decay. Here, we assume advection velocity ('V') is zero. Diffusive mixing coefficient of hillcrests are shown in the figure, and average hillslope values at each site are 0.28 ± 0.05 cm^2/yr at BG and 0.15 ± 0.02 cm^2/yr at WB. Inventories (c, d) of $^{210}Pb_{excess}$ and ^{137}Cs for downslope soils at low-elevation BG (gray squares) and high-elevation WB (black circles). Inventory data points reflect those calculated from individual soil profiles and activities of additional bulk soil samples gathered downslope. (c) Nuclide inventories at high elevation are lower at high slopes; however, no statistically significant correlation exists. (d) At BG, inventories do not change markedly, while at WB, nuclide inventories decrease with distances downslope and increasing contributing area.

Author's personal copy

discharge (e.g. Kaste et al., 2006). This correlation, in agreement with the observation of rills, shows that overland flow plays an important role in soil transport at WB.

While overland flow may play a dominant role in sediment transport at WB, it likely has little impact on soil production. Spatial patterns of soil production are distinctly different at the two sites (Fig. 5a), and an apparent soil production function at low elevation is consistent with production mechanisms such as rooting and bioturbation, which are expected to be depth dependent (e.g. Heimsath et al., 1997, 2000, 2005). It is possible that the absence of a trend between P_{soil} and depth at the higher elevation, WB, site is due to soil depths temporarily out of local steady state; and, indeed, the two deepest samples are anomalies in the sampled transect. More likely, the absence of depth-dependent soil production at WB (Fig. 5a) and the differences in hillslope patterns of erosion and weathering (Fig. 5b,c) suggest that a different mechanism is dominant at the high elevation site. With average annual temperatures of 3.9 °C, freeze–thaw may occur at WB; however, this process is also likely depth dependent (e.g. Anderson, 2002). Furthermore, freeze–thaw is likely not a dominant soil production or transport process given that rills are prominent on the land surface and that soil thicknesses typically exceed one meter. Biotite hydration and oxidation may occur at depth in saturated soils during spring snowmelt; however, our data do not speak directly to this mechanism and further research is needed to explain what processes ultimately create these thick high elevation soils.

The steady-state distribution of $^{210}Pb_{ex}$ in soils can be described by solving the traditional advection–diffusion model (e.g. DeMaster and Cochran, 1982), where the amount of $^{210}Pb_{ex}$ in a particular volume of soil (A, in Bq cm^{-3}) is controlled by the initial amount (A_0), an advection term, which is defined here as downward leaching of nuclides sorbed to colloidal materials, as expressed above in Eqn (14). Radioactive equilibrium is a reasonable assumption at our sites: they have remained free from anthropogenic disturbance for at least 3 half-lives of ^{210}Pb, precipitation (which can control deposition) has remained relatively constant during the 20th century, and measured total inventories are consistent with those predicted by deposition models. By modeling the distribution of a single isotope in the soil column, it is not possible to solve for unique values of v and D, and it is unrealistic to ignore either leaching or diffusion-like processes in soils. While our goal is to quantify D to measure sediment mixing, we need to constrain advection that might occur. For this, we use the distribution of weapons-derived nuclides (^{137}Cs and ^{241}Am) in the soil profile, which had a pulse-like input to soils during the 1950s and 1960s, with a strong global depositional maxima in 1963–1964 (US ERDA, 1977). Using the precise position of the subsurface concentration maxima of weapons-fallout in our soils, we determine v (Fig. 8).

While advection–diffusion models are the most common method for describing the depth distribution of fallout nuclides (Walling et al., 1999 and references therein), an alternative model for describing radionuclide

Author's personal copy

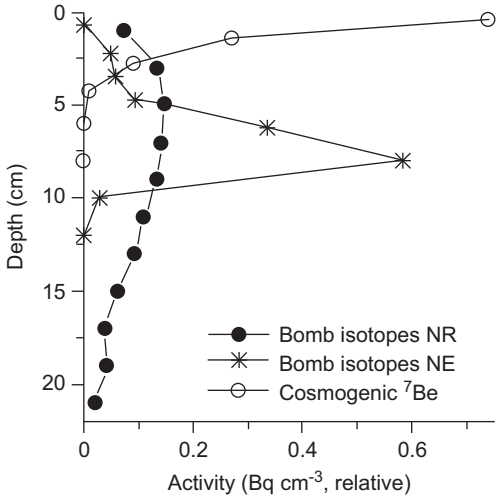

FIGURE 8 Depth profiles of cosmogenic ^{7}Be and weapons-fallout isotopes at New England (NE) and Nunnock River, Bega Valley (BV) field sites as described in Kaste et al. (2007). ^{7}Be is largely (>80%) retained in the upper 2 cm of soil. Weapons-fallout isotopes display a sharp subsurface peak at NE because of limited mixing; at BV, similar isotopes are more dispersed presumably from bioturbation. We calculate v by using the position of the subsurface maxima and assume that it tracks the 1963 deposition spike: v ranged from 0.1 to 0.2 at NE, and from 0.08 to 0.12 at BV and MC.

depth profiles may be required for sites that do not fall into the reasonably well-constrained conceptual framework outlined above. For example, in New England (NE) >70% of the total $^{210}Pb_{ex}$ inventory resides in organic matter and the soils we examined showed no evidence of physical mixing. These, therefore, provided an important comparison with the well-mixed upland soils that are more typical for the landscapes selected for our work. Organic matter decomposition must govern the concentration depth profiles of $^{210}Pb_{ex}$ in O horizons to some extent, since the half-life of ^{210}Pb is nearly an order of magnitude higher than the half-life or organic matter. As organic matter decomposes, $^{210}Pb_{ex}$ concentrations will increase from relative carbon loss. A modified constant initial concentration (CIC) model (developed elsewhere for sedimentary environments; Appleby and Oldfield, 1992) can be applied to our measured $^{210}Pb_{ex}$ profiles, assuming that litterfall and ^{210}Pb flux are relatively constant over time, and that the contribution of root mass in the O horizon is relatively low. We posit that the only difference between the CIC model and our data is an exponential-based organic matter decomposition function. The decomposition functions that best explained our observed $^{210}Pb_{ex}$ concentration-depth profiles from NE can be evaluated using additional data on C cycling developed by others for similar forests (Currie and Aber, 1997; Berg, 2000).

We maximized the fit on the upper 15–20 cm of soil, the portion of the soil with the majority of the nuclide inventory and the portion most likely to be influenced by organisms. At NR and TV, the advection–dispersion model described the $^{210}Pb_{ex}$ profiles well, as total misplaced inventory was typically <18%. Dispersion coefficients can then be used to calculate mixing time constants τ for a soil of thickness L ($\tau = L^2D^{-1}$). A soil 35 cm thick at NR is "turned over", or mixed every 1200 y, and a similar thickness of soil at TV is

Author's personal copy

mixed every 660 y. If we use the mixing timescale for a soil of 35-cm thickness at NR and assume that a particle travels 0.5 L during τ, we calculate grain-scale vertical displacement velocities of 1–2 cm per century. Surprisingly, these values are relatively consistent with the 1–4 cm per century grain-scale velocities calculated at the same site by luminescence dating (Heimsath et al., 2002).

In contrast with NR and TV, a simple advection–dispersion model did not fit the data well in NE; our best model-data fits had misplaced inventory >30% (Fig. 9). In addition, the D values calculated here were on the order of 1 $cm^2\ y^{-1}$, a rate inconsistent with the preservation of the weapons spike (Fig. 8). Because the upper 5–10 cm of soil is the O horizon at our NE sites, which is usually >70% organic matter and very porous (~75%), the initial infiltration of rainwater during intense storms could result in subsurface $^{210}Pb_{ex}$ peaks (Fig. 9c). Profiles of cosmogenic ^{7}Be would capture this process well because of its short half-life and its association with large rain events (Olsen et al., 1985). However, episodic vertical transport that might accompany intense precipitation events appears to be low at all three sites: ^{7}Be activity declines rapidly with depth and the upper 2 cm of soil typically retains >80% of the ^{7}Be inventory (Fig. 8). ^{7}Be was completely retained in the upper 1–2 cm of soil at NR and TV.

Physical soil mixing rates determined with short-lived isotopes correlate well with physical denudation rates measured by others (Fig. 10). Specifically, short-term soil mixing rates are highest at TV, where Heimsath et al. (1997) reported landscape denudation rates approaching 0.1 mm y^{-1} from cosmogenic nuclide analysis. On the other hand, physical denudation rates measured by

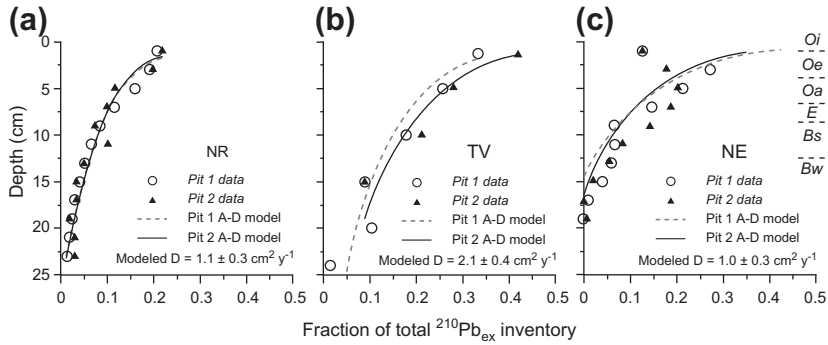

FIGURE 9 $^{210}Pb_{ex}$ data and advection–diffusion (a–d) model given by Eqn (14); v was calculated using weapons-derived isotopes (Fig. 8); we then solved for a D that best matched our data: 80–90% agreement at BV and Point Reyes, Marin County (MC), sites of Heimsath et al. (2005), in NE fits were typically <70%. Appendix 1 of Kaste et al. (2007) has more details on NE fits. Soil horizons observed at New England shown on far right; no equivalent horizon boundaries exist at Bega Valley and Marin County. Oi, fresh litter; Oe, moderately decomposed litter; Oa, humus; E, strongly leached zone; Bs, zone with strong illuviation of iron oxides; Bw, chemically altered zone with weak illuviation.

Author's personal copy

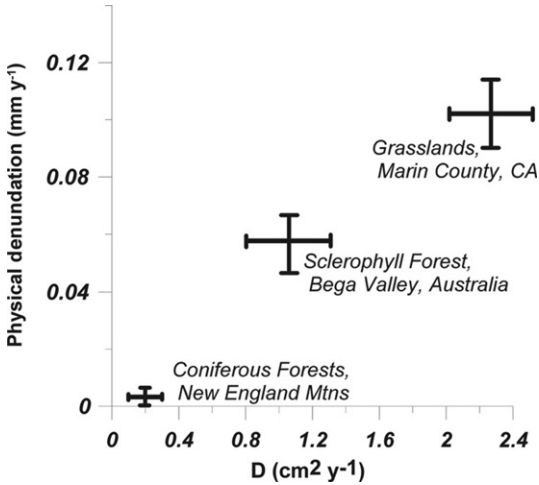

FIGURE 10 Short-term physical soil mixing rates calculated in Kaste et al. (2007) vs. landscape denudation measured by sediment traps and cosmogenic isotopes in Heimsath et al. (1997; 2000). A maximum D of 0.2 cm^2 yr^{-1} for NE soils was determined by using the shape of the ^{241}Am peak (plots similar to Fig. 7) and an instantaneous pulse-like input source assumption.

sediment traps in central NE are orders of magnitude lower (Likens and Bormann, 1995), and we conclude from our nuclide profiles that short timescale diffusion-like processes play a negligible role in mixing the soil layer here. This suggests that relatively short-term soil mixing processes may limit erosion rates, and that there is a rough steady state between the continuous processes of soil mixing and long-term landscape evolution across contrasting field settings. These results are interesting because tree-throw and landslides, which can occur episodically on timescales >100 y, are thought to be a significant sediment-transport mechanism (Dietrich et al., 2003). Because the $^{210}Pb_{ex}$ depth-concentration profiles are not described well with an A–D model, our work demonstrates quantitatively that freeze–thaw does not drive diffusion-like soil mixing in New England. The persistence of an insulating snowpack cover during the winter months probably minimizes the frequency of soil freezing cycles here (Likens and Bormann, 1995). The presence of a fibrous, porous organic horizon in northern NE that undergoes short-term mixing only via decomposition (and not random stirring) may protect mineral soil, and probably limits physical denudation here. Using short-lived isotopes in this way demonstrates quantitatively how process rates can vary in different geological settings on a timescale that is traditionally difficult to capture. Furthermore, we show that short-term diffusion-like processes are significant, and can play an important role in landscape evolution and the fate of any element delivered to the land surface.

4.4. Parent Material Strength

I now attempt to pull together all of the above results and discussion into a final field-based measurement that is intended to provide a key mechanistic parameter for hillslope evolution. At several of our field sites, we used both

Author's personal copy

the cone penetrometer and the shear vane described above to quantify parent material resistance to shear. Other studies explored the correlation between these two instruments at different sites (Bachmann et al., 2006; Zimbone et al., 1996). Bachmann et al. specifically addressed the appropriateness of using a dynamic-cone penetrometer in soils to measure a horizontal shear stress that is a relative measure for the in situ strength state. The shear strength of a soil is directly related to the normal stress applied (McKyes, 1989); therefore, an instrument that applies a force normal to the surface enables the estimate a relative shear strength. In fact, Bachmann et al. (2006) found that the vertically measured compression strength (strikes/cm) obtained at the final soil depth linearly related to the horizontal shear stress measured by the shear vane tester. We confirmed this with our own measurements and determined a linear fit between dynamic-cone penetrometer and shear vane tester measurements that we used to convert strikes/cm from the cone penetrometer to kilopascals (Fig. 11).

Using both the shear vane and the cone penetrometer in soil pits dug across three different field sites first reported elsewhere (Heimsath et al., 2000, 2005, 2006, 2012), we quantify depth dependence for parent material strength (Fig. 12a). For each of the three field sites used for this aspect of our work, we occupied the soil pits used for our cosmogenic nuclide and chemical weathering sampling studies and measured the competence of the parent material immediately beneath the mobile soil layer. The shallowest soils were observed in the rugged landscape of the San Gabriel Mountains, CA (SG) (Heimsath et al., 2012), where there is a relatively steep increase in parent material strength with increasing soil depth (black diamonds in Fig. 12a). Samples from

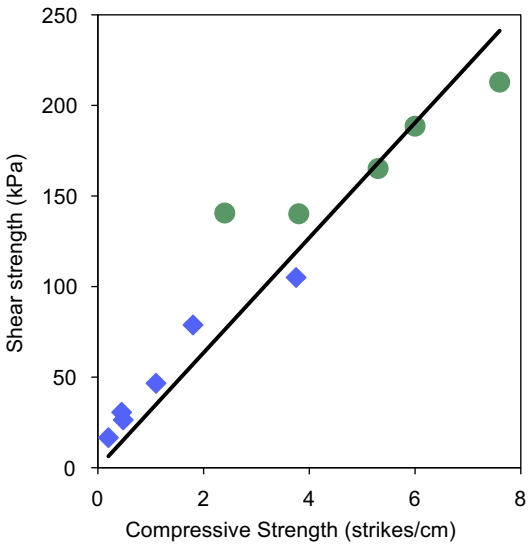

FIGURE 11 Linear relationship between shear vane tester and dynamic-cone penetrometer. Good linear fit confirms principal stress theory such that the vertically measured compression strength (strikes/cm) obtained at the final soil depth is identical in size with the horizontal shear stress measured by the shear vane tester. Green filled circles from Byersdorfer (2006) and blue filled diamonds from Johnson (2008). Black line is fit to both data sets, shear strength (kPa) = 32 × compressive strength (strikes/cm); $R^2 = 0.86$. *(Color version online)*

Author's personal copy

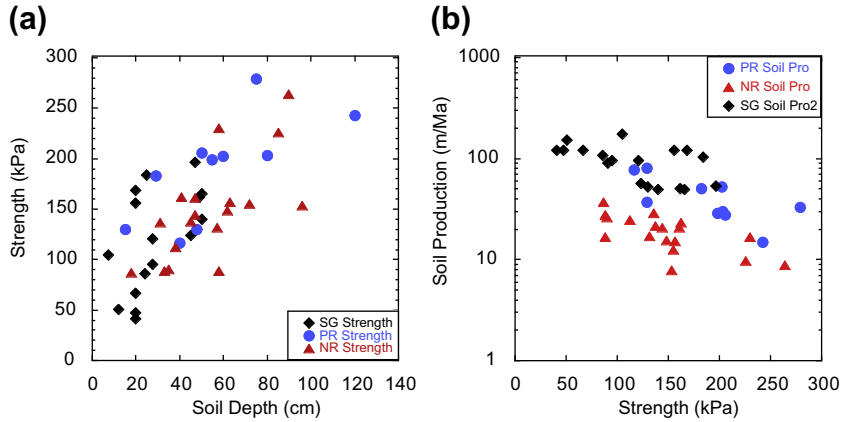

FIGURE 12 (a) Shear strength of the parent material beneath the active soil layer for three of the field sites discussed here: San Gabriel Mountains (SG), California, described in DiBiase et al. (2010) and Heimsath et al. (2012); Point Reyes (PR), California, just north of photograph in Figure 1 and discussed in Heimsath et al. (2005); Nunnock River (NR), Bega Valley, Australia, described initially in Heimsath et al. (2000) and several papers since then. Strength of the saprolite is measured with both a shear vane and a cone penetrometer across the full range of soil depths – strength vs. depth and increases across all sites with increasing soil thickness; (b) soil production rates calculated with the soil production functions reported in Heimsath et al. (in review) for SG, Heimsath et al. (2005 for PR) and Heimsath et al. (2000) for NR vs. the shear strength measured beneath the same soil thicknesses as shown in (a). *(Color version online)*

the Nunnock River, Australia, site (Heimsath et al., 2000, 2006) (NR; red triangles) overlay the SG measurements and the Point Reyes, California, samples (PR; blue circles) (Heimsath et al., 2005). Each of the three field sites shows a distinct increase of parent material strength with increasing overlying soil thickness. Additionally, when taken together, these data suggest a broader relationship between parent material resistance to shear and the soil depth that mantles the sample locations.

In related work that I did not expand upon in this chapter, we showed that the chemical weathering rates in saprolite decreased beneath increasing soil thicknesses (Burke et al., 2007, 2009). Those findings were counterintuitive to our observations of more highly weathered saprolite corresponding to thicker overlying soil depths, but made sense when examined from the perspective that the higher soil production rates found beneath shallower soils should correspond to higher chemical weathering rates (Dixon et al., 2009a,b). The impact on physical weathering processes of the slower weathering rate beneath thicker soils is quantified with our measurements of parent material strength (Fig. 12a), and the observation of higher clay contents being found beneath thicker soils (Burke et al., 2009). We suggest that these higher clay contents and the more deeply weathered saprolites (i.e. with higher chemical indices of alteration as discussed in Burke et al. (2007)) are actually more resistant to physical shear,

Author's personal copy

rather than being more easily mobilized by physical weathering processes. While this may seem to be the opposite of what we might predict, the observations from a wide range of weathered granite saprolites, across very different field areas, seem to indicate a very clear relationship between parent material competence and overlying soil depth.

Exploring the implications of this relationship between strength and overlying soil thickness is the final connection made with the different measurements summarized in this chapter. Each of the field sites discussed, as well as several that were not, has shown clear soil production functions quantified using cosmogenic nuclides (^{10}Be and, in some cases, ^{26}Al). Eqn (15) reports one such equation for the Point Reyes (PR), California, field area. Similar equations were reported for the NR (Heimsath et al., 2000, 2006) and SG (Heimsath et al., 2012) field sites and are not repeated here. Each of these soil production functions defines a strikingly clear decrease of soil production rates with increasing soil thickness. Fig. 12a shows a clear increase in strength of the same parent material used to quantify the soil production functions with increasing soil thickness. If we use the relationships quantified with our independent field measurements we can plot soil production as a function of parent material strength (Fig. 12b) to suggest an inferred dependence between soil production and competence. Data from each of the three field sites reveal separate, but overlapping, relationships, and the data taken together suggest that there may be a broadly applicable dependence between parent material strength and soil production processes. Although the relationship suggested by this figure makes intuitive sense, it has never been documented before.

5. CONCLUSION

The relationships suggested by Fig. 12 provide an exciting way to tie together the very different aspects of quantifying hillslope processes presented in this chapter. These aspects appear to be broadly applicable to landscapes that do not experience glacial processes and have not had significant eolian deposition and we deliberately focus on the physically mobile soils that form a thin mantle across upland landscapes. These studies, and the summary provided by this chapter, also provide some clear paths that we are attempting to follow to help more fully understand how hilly and mountainous landscapes evolve under different conditions. Our conceptual framework for examining such landscapes connects denudation, driven by external forcing, to both physical and chemical processes acting on the soils and the underlying parent material. Soil production processes are primarily physical (burrowing fauna, disrupting flora, freeze–thaw, and wetting–drying), and also depend inherently on the chemical weathering experienced by the parent material. We have found that both soil production and chemical weathering rates decrease with increasing soil thickness. We also show that the extent, or degree, of weathering increases beneath thicker soils and suggest that this increase in clay content contributes to

Author's personal copy

the increase in parent material competence observed beneath thicker soils. This increase in competence corresponds to a decrease in soil production rates at the same sites and we speculate that quantifying clay content more completely will lead to a more definitive connection.

Processes transporting the soil play an important role in connecting the incoming precipitation with the underlying parent material; namely, we have used short-lived fallout-derived isotopes to quantify the physical mixing processes that are active across these landscapes. At all the sites where we have made these measurements, we have documented a transition from dominant physical mixing in the soil column to a dominance of overland flow with increasing distance downslope. This transition from mixing to overland flow corresponds to the transition from thin to thick soils because all of our field sites have increasing soil depths downslope. The increase in overland flow processes downslope may mean that the parent material beneath thicker soils is in contact with soil water that has traveled farther through soil and is, therefore, not as able to weather as the water reacting with the parent material beneath the thinner, upslope soils. While this suggestion is speculative at best, it presents a very clear link between hillslope hydrological processes acting across these landscapes and the physical and chemical processes that I have summarized in this chapter. If we can make all the observations presented in this chapter on landscapes where the hillslope hydrology is well known, or vice versa, there will be excellent opportunities to test this speculation and lead to a truly comprehensive understanding of how upland landscapes evolve.

ACKNOWLEDGMENTS

This chapter reflects the enormous amount of work done by my graduate students over the last decade. Jim Kaste helped hone and develop the short-lived isotope methodology applied here to quantifying soil transport processes and rates. Ben Burke helped initiate the studies connecting soil production rates and processes with saprolite weathering. Jean Dixon took all these methods further and integrated them with extensive work on quantifying the chemical weathering signals on upland landscapes. Elizabeth Johnson and Joel Beyersdorfer lifted the heavy cone penetrometer across many hillslopes and contributed to the strength studies. Recent application of all of these methods in the San Gabriel Mountains benefited greatly from the work of Roman DiBiase, Matt Jungers, and Josh Landis. My sincere thanks to all of them.

REFERENCES

Ahnert, F., 1967. The role of the equilibrium concept in the interpretation of landforms of fluvial erosion and deposition. In: Macar, P. (Ed.), L'evolution Des Versants. University of Liege, Liege, pp. 23–41.

Ahnert, F., 1976. Brief description of a comprehensive three-dimensional process-response model of landform development. Zeitschrift fur Geomorphologie, Supp. Band 25, 29–49.

Amundson, R., Richter, D.D., Humphreys, G.S., Jobbagy, E.G., Gaillardet, J., 2007. Coupling between biota and earth materials in the critical zone. Elements 3 (5), 327–332.

Author's personal copy

Anderson, R.S., Humphrey, N.F., 1989. Interaction of weathering and transport processes in the evolution of arid landscapes. In: Cross, T.A. (Ed.), Quantitative Dynamic Stratigraphy. Prentice-Hall, Englewood Cliffs, N.J, pp. 349–361.

Anderson, R.S., 1994. Evolution of the santa cruz mountains, California, through tectonic growth and geomorphic decay. J. Geophys. Res. Solid Earth 99 (B10), 20161–20179.

Anderson, R.S., 2002. Modeling the tor-dotted crests, bedrock edges, and parabolic profiles of high alpine surfaces of the Wind River Range, Wyoming. Geomorphology 46, 35–58.

Anderson, S.P., Dietrich, W.E., 2001. Chemical weathering and runoff chemistry in a steep headwater catchment. Hydrolog. Process. 15 (10), 1791–1815.

Anderson, S.P., Blum, J.D., Brantley, S.L., Chadwick, O., Chorover, J., Derry, L.A., Drever, J.I., Hering, J.G., Kirchner, J.W., Kump, L.R., Richter, D.D., White, A.F., 2004. Proposed initiative would study earth's weathering engine. EOS Trans. Am. Geophys. Union 85 (28), 265–269.

Anderson, S.P., von Blanckenburg, F., White, A.F., 2007. Physical and chemical controls on the critical zone. Elements 3 (5), 315–319.

Appleby, P.G., Oldfield, F., 1992. Application of lead-210 to sedimentation studies. In: Ivanovich, M., Harmon, R.S. (Eds.), Uranium-series Disequilibrium. Oxford University Press.

Bachmann, J., Contreras, K., Hartge, K.H., MacDonald, R., 2006. Comparison of soil strength data obtained in situ with penetrometer and with vane shear test. Soil Tillage Res. 87, 112–118.

Balco, G., Stone, J.O., Lifton, N.A., Dunai, T.J., 2008. A complete and easily accessible means of calculating surface exposure ages or erosion rates from ^{10}Be and ^{26}Al measurements. Quaternary Geochronology 3, 174–194.

Berg, B., 2000. Litter decomposition and organic matter turnover in northern forest soils. Forest Ecol. Manag. 133, 13–22.

Bierman, P.R., 2004. Rock to sediment – slope to sea with Be-10 – rates of landscape change. Annu. Rev. Earth Planet. Sci. 32, 215–255.

Black, T.A., Montgomery, D.R., 1991. Sediment transport by burrowing animals, Marin county, California. Earth Surf. Process. Landforms 16, 163–172.

Bonniwell, E.C., Matisoff, G., Whiting, P.J., 1999. Determining the times and distances of particle transit in a mountain stream using fallout radionuclides. Geomorphology 27, 75–92.

Brantley, S.L., Goldhaber, M.B., Ragnarsdottir, K.V., 2007. Crossing disciplines and scales to understand the critical zone. Elements 3 (5), 307–314.

Braun, J., Heimsath, A.M., Chappell, J., 2001. Sediment transport mechanisms on soil-mantled hillslopes. Geology 29, 683–686.

Brimhall, G.H., Dietrich, W.E., 1987. Constitutive mass balance relations between chemical composition, volume, density, porosity, and strain in metasomatic hydrochemical systems: results on weathering and pedogenesis. Geochim. Cosmochim. Acta 51, 567–587.

Brimhall, G.H., Chadwick, O.A., Lewis, C.J., Compston, W., Williams, I.S., Danti, K.J., Dietrich, W.E., Power, M.E., Hendricks, D., Bratt, J., 1992. Deformational mass transport and invasive processes in soil evolution. Science 255, 695–702.

Brown, R.B., Cutshall, N.H., Kling, G.F., 1981a. Agricultural erosion indicated by Cs-137 redistribution 1. Levels and distribution of Cs-137 activity in soils. Soil Sci. Soc. Am. J. 45 (6), 1184–1190.

Brown, R.B., Kling, G.F., Cutshall, N.H., 1981b. Agricultural erosion indicated by Cs-137 redistribution. 2. Estimates of erosion rates. Soil Sci. Soc. Am. J. 45 (6), 1191–1197.

Burke, B.C., Heimsath, A.M., White, A.F., 2007. Coupling chemical weathering with soil production across soil-mantled landscapes. Earth Surf. Process. Landforms 32, 853–873.

Author's personal copy

Burke, B.C., Heimsath, A.M., Dixon, J.L., Chappell, J., Yoo, K., 2009. Weathering the escarpment: chemical and physical rates and processes, South-Eastern Australia. Earth Surf. Process. Landforms 34, 768–785.

Burkins, D.L., Blum, J.D., Brown, K., Reynolds, R.C., Erel, Y., 1999. Chemistry and mineralogy of a granitic, glacial soil chronosequence, Sierra Nevada Mountains, California. Chem. Geol. 162 (1), 1–14.

Buss, H.L., Brantley, S.L., Sak, P.B., White, A.F., 2004. Mineral dissolution at the grantie-saprolite interface. In: Wanty, R.B., Seal, R.R.I. (Eds.), 11th International Symposium on Water-Rock Interaction 11. Taylor and Francis, Saratoga Springs, NH, pp. 819–823.

Buss, H.L., Sak, P.B., Webb, S.M., Brantley, S.L., 2008. Weathering of the rio blanco quartz diorite, Luquillo Mountains, Puerto Rico: Coupling oxidation, dissolution, and fracturing. Geochim. Cosmochim. Acta 72, 4488–4507.

Byersdorfer, J.P., 2006. Correlating saprolite strength, soil production rate and chemical weathering in granitic terrain: Point Reyes, CA and Nunnock River, Australia. MS Thesis, Dartmouth College, Department of Earth Sciences.

Cambray, R.S., Playford, K., Lewis, F.N.J., Carpenter, R.C., 1989. Radioactive Fallout in Air and Rain: Results to the End of 1988. UK Atomic Energy Authority, Report no. AERE-R 10155, Environ. Med. Sci. Div. Harwell Lab, Oxfordshire.

Carson, M.A., Kirkby, M.J., 1972. Hillslope Form and Process. Cambridge University Press, New York, p. 475.

Cox, N.J., 1980. On the relationship between bedrock lowering and regolith thickness. Earth Surf. Process. Landforms 5, 271–274.

Currie, W.S., Aber, J.D., 1997. Modeling leaching as a decomposition process in humid montane forests. Ecology 78 (6), 1844–1860.

Dahlgren, R.A., Boettinger, J.L., Huntington, G.L., Amundson, R.G., 1997. Soil development along an elevational transect in the western Sierra Nevada, California. Geoderma 78, 207–236.

DeMaster, D.J., Cochran, J.K., 1982. Particle mixing rates in deep-sea sediments determined from excess ^{210}Pb and ^{32}Si profiles. Earth Planet. Sci. Lett. 61, 257–271.

DiBiase, R.A., Whipple, K.X., Heimsath, A.M., Ouimet, W.B., 2010. Landscape form and millennial erosion rates in the San Gabriel Mountains, CA. Earth Planet. Sci. Lett. 289, 134–144.

Dietrich, W.E., Perron, J.T., 2006. The search for a topographic signature of life. Nature 439, 411–418.

Dietrich, W.E., et al., 2003. Geomorphic transport laws for predicting landscape form and dynamics. In: Wilcock, P., Iverson, R. (Eds.), Prediction in Geomorphology. American Geophysical Union, Washington, D.C, pp. 103–132.

Dietrich, W.E., Reiss, R., Hsu, M.-L., Montgomery, D.R., 1995. A process-based model for colluvial soil depth and shallow landsliding using digital elevation data. Hydrolog. Process. 9, 383–400.

Dixon, J.L., Heimsath, A.M., Amundson, R., 2009a. The Critical Role of Climate and Saprolite Weathering in Landscape Evolution. Earth Surf. Process. Landforms 34, 1507–1521.

Dixon, J.L., Heimsath, A.M., Kaste, J., Amundson, R., 2009b. Climate-driven processes of hillslope weathering. Geology 37, 975–978.

Dörr, H., 1995. Application of Pb-210 in Soils. J. Paleolimnol. 13 (2), 157–168.

Fleming, R.W., Johnson, A.M., 1975. Rates of seasonal creep of silty clay soil. Q. J. Eng. Geol. 8, 1–29.

Fletcher, R.C., Buss, H.L., Brantley, S.L., 2006. A spheroidal weathering model coupling porewater chemistry to soil thicknesses during steady-state denudation. Earth Planet. Sci. Lett. 244, 444–457.

Author's personal copy

Fornes, W.L., Whiting, P.J., Wilson, C.G., Matisoff, G., 2005. ^{137}Cs-derived erosion rates in an agricultural setting: the effects of model assumptions and management practices. Earth Surf. Process. Landforms 30 (9), 1181–1189.

Frazier, C.S., Graham, R.C., 2000. Pedogenic transformation of fractured granitic bedrock, southern California. Soil Sci. Soc. Am. J. 64, 2057–2069.

Furbish, D.J., 2003. Using the dynamically coupled behavior of land-surface geometry and soil thickness in developing and testing hillslope evolution models. In: Wilcock, P., Iverson, R. (Eds.), Prediction in Geomorphology, vol. 135. American Geophysical Union, Washington, D.C, Geophysical Monograph, pp. 169–182.

Furbish, D.J., Haff, P.K., Dietrich, W.E., Heimsath, A.M., 2009. Statistical description of slope-dependent soil transport and the diffusion-like coefficient. J. Geophys. Res. 114, F00A05, doi: 10.1029/2009JF001267.

Gabet, E.J., 2000. Gopher bioturbation: field evidence for nonlinear hillslope diffusion. Earth Surf. Process. Landforms 25, 1419–1428.

Gabet, E.J., Reichman, O.J., Seabloom, E.W., 2003. The effects of bioturbation on soil processes and sediment transport. Ann. Rev. Earth Planet. Sci. 31, 249–273.

GEONOR, Instructions for Use, Inspection Vane Tester, H-60. GEONOR, INC, Milford, PA. Available at http://www.geonor.com/field_vane_testing.html

Gilbert, G.K., 1877. Report on the Geology of the Henry Mountains (Utah). United States Geological Survey, Washington, D.C.

Gilbert, G.K., 1909. The Convexity of Hilltops. Journal of Geology 17 (4), 344–350.

Green, E.G., Dietrich, W.E., Banfield, J.F., 2006. Quantification of chemical weathering rates across an actively eroding hillslope. Earth Planet. Sci. Lett. 242, 155–169.

Hack, J.T., 1960. The interpretation of erosional topography in humid temperate regions. Am. J. Sci. 258A, 80–97.

He, Q., Walling, D.E., 2003. Testing distributed soil erosion and sediment delivery models using Cs-137 measurements. Hydrolog. Process. 17 (5), 901–916.

He, Q., Walling, D.E., 1996. Interpreting particle size effects in the adsorption of Cs-137 and unsupported Pb-210 by mineral soils and sediments. J. Environ. Radioact. 30 (2), 117–137.

Heimsath, A.M., 2006. Eroding the land: steady-state and stochastic rates and processes through a cosmogenic lens. Geol. Soc. Am. Spec. Pap. 415, 111–129.

Heimsath, A.M., Chappell, J., Fifield, K., 2010. Eroding Australia: Rates and Processes from Bega Valley to Arnhem Land. Geological Society, London. Special Publications, 346: 225–241.

Heimsath, A.M., Chappell, J., Dietrich, W.E., Nishiizumi, K., Finkel, R.C., 2000. Soil production on a retreating escarpment in southeastern Australia. Geology 28, 787–790.

Heimsath, A.M., Chappell, J., Dietrich, W.E., Nishiizumi, K., Finkel, R.C., 2001a. Late Quaternary erosion in southeastern Australia: a field example using cosmogenic nuclides. Quaternary Int. 83–5, 169–185.

Heimsath, A.M., Chappell, J., Finkel, R.C., Fifield, L.K., Alimanovic, A., 2006. Escarpment erosion and landscape evolution in southeastern Australia. v. Penrose Conference Series. Geol. Soc. Am. Spec. Pap. 398, 173–190.

Heimsath, A.M., Chappell, J., Spooner, N.A., Questiaux, D., 2002. Creeping soil. Geology 30, 111–114.

Heimsath, A.M., Dietrich, W.E., Nishiizumi, K., Finkel, R.C., 1997. The soil production function and landscape equilibrium. Nature 388, 358–361.

Heimsath, A.M., Dietrich, W.E., Nishiizumi, K., Finkel, R.C., 1999. Cosmogenic nuclides, topography, and the spatial variation of soil depth. Geomorphology 27, 151–172.

Author's personal copy

Heimsath, A.M., Dietrich, W.E., Nishiizumi, K., Finkel, R.C., 2001b. Stochastic processes of soil production and transport: erosion rates, topographic variation, and cosmogenic nuclides in the Oregon coast range. Earth Surf. Process. Landforms 26, 531–552.

Heimsath, A.M., Furbish, D.J., Dietrich, W.E., 2005. The illusion of diffusion: field evidence for depth-dependent sediment transport. Geology 33, 949–952.

Heimsath, A.M., Hancock, G.R., Fink, D., 2009. The 'humped' soil production function: eroding Arnhem Land, Australia. Earth Surf. Process. Landforms 34, 1674–1684.

Heimsath, A.M., DiBiase, R.A., Whipple, K.X., 2012. Soil production limits and the transition to bedrock dominated landscapes. Nature Geoscience 5 (5), 210–214.

Herrick, J.E., Jones, T.L., 2002. A dynamic cone penetrometer for measuring soil penetration resistance. Soil Sci. Soc. Am. J. 66, 1320–1324.

Hole, F.D., 1981. Effects of animals on soil. Geoderma 25, 75–112.

Jiao, J.J., Wang, X.-S., Nandy, S., 2005. Confined groundwater zone and slope instability in weathered igneous rocks in Hong Kong. Eng. Geol. 80, 71–92.

Johnson-Maynard, J., Anderson, M.A., Green, S., Graham, R.C., 1994. Physical and hydraulic-properties of weathered granitic rock in Southern California. Soil Sci. 158 (5), 375–380.

Johnson, E.R., 2008. Rocks Matter: Exploring the Intersection of Lithology and Tectonics. MS Thesis, Dartmouth College Department of Earth Sciences.

Jones, D.P., Graham, R.C., 1993. Water-holding characteristics of weathered granitic rock in chaparral and forest ecosystems. Soil Sci. Soc. Am. J. 57 (1), 256–261.

Kaste, J.M., Heimsath, A.M., Bostick, B.C., 2007. Short-term soil mixing quantified with fallout radionuclides. Geology 35, 243–246.

Kaste, J.M., Heimsath, A.M., Hohmann, M., 2006. Quantifying sediment transport across an undisturbed prairie landscape using cesium-137 and high resolution topography. Geomorphology 76, 430–440.

Kew, G., Gilkes, R., 2006. Classification, strength and water retention characteristics of lateritic regolith. Geoderma 136, 184–198.

Lal, D., 1991. Cosmic ray labeling of erosion surfaces: in situ nuclide production rates and erosion models. Earth Planet. Sci. Lett. 104, 424–439.

Lamb, M.P., Scheingross, J.S., Amidon, W.H., Swanson, E., Limaye, A., 2011. A Model for Fire-Induced Sediment Yield by Dry Ravel in Steep Landscapes. J. Geophys. Res. 116, F03006, doi:10.1029/2010JF001878.

Lebedeva, M.I., Fletcher, R.C., Balashov, V.N., Brantley, S.L., 2007. A reactive diffusion model describing transformation of bedrock to saprolite. Chem. Geol. 244, 624–645.

Likens, G.E., Bormann, F.H., 1995. Biogeochemistry of a Forested Ecosystem. Springer-Verlag, New York, p. 160.

Lowrance, R., McIntyre, S., Lance, C., 1988. Erosion and deposition in a field forest system estimated using cesium-137 activity. J. Soil Water Conservat. 43 (2), 195–199.

Lutz, H.J., Griswold, F.S., 1939. The influence of tree roots on soil morphology. Am. J. Sci. 258, 389–400.

Lutz, H.J., 1940. Disturbance of forest soil resulting from the uprooting of trees. Bull. Yale Univ. Sch. Forest 45, 1–37.

Lutz, H.J., 1960. Movement of rocks by uprooting of forest trees. Am. J. Sci. 258, 752–756.

Matisoff, G., Bonniwell, E.C., Whiting, P.J., 2002a. Radionuclides as indicators of sediment transport in agricultural watersheds that drain to Lake Erie. J. Environ. Qual. 31 (1), 62–72.

Matisoff, G., Bonniwell, E.C., Whiting, P.J., 2002b. Soil erosion and sediment sources in an Ohio watershed using beryllium-7, cesium-137, and lead-210. J. Environ. Qual. 31 (1), 54–61.

Author's personal copy

Matisoff, G., Ketterer, M.E., Wilson, C.G., Layman, R., Whiting, P.J., 2001. Transport of rare earth element-tagged soil particles in response to thunderstorm runoff. Environ. Sci. Technol. 35 (16), 3356–3362.

Matsuoka, N., 1990. The rate of bedrock weathering by frost action: field measurements and a predictive model. Earth Surf. Process. Landforms 15, 73–90.

Matsuoka, N., Moriwaki, K., 1992. Frost heave and creep in the sor rondane mountains. Arctic Antarct. Alpine Res. 24, 271–280.

McKean, J.A., Dietrich, W.E., Finkel, R.C., Southon, J.R., Caffee, M.W., 1993. Quantification of soil production and downslope creep rates from cosmogenic ^{10}Be accumulations on a hillslope profile. Geology 21 (4), 343–346.

McKyes, E., 1989. Agricultural Engineering Soil Mechanics. In: Developments in Agricultural Engineering, vol. 10. Elsevier, Amsterdam, p. 292.

Minasny, B., McBratney, A.B., 1999. A rudimentary mechanistic model for soil production and landscape development. Geoderma 90 (1–2), 3–21.

Minasny, B., McBratney, A.B., 2001. A rudimentary mechanistic model for soil formation and landscape development II. A two-dimensional model incorporating chemical weathering. Geoderma 103, 161–179.

Mitchell, P., 1988. The influences of vegetation, animals and micro-organisms on soil processes. In: Viles, H.A. (Ed.), Biogeomorphology. Basil Blackwell, New York, pp. 43–82.

Montgomery, D.R., 2007. Soil erosion and agricultural sustainability. Proc. Natl. Acad. Sci. U S A 104 (33), 13268–13272.

Mudd, S.M., Furbish, D.J., 2006. Using chemical tracers in hillslope soils to estimate the importance of chemical denudation under conditions of downslope sediment transport. J. Geophys. Res. Earth Surf. 111 (F2).

Norman, S.A., Schaetzl, R.J., Small, T.W., 1995. Effects of slope angle on mass movements by tree uprooting. Geomorphology 14, 19–27.

O'Farrell, C.R., Heimsath, A.M., Kaste, J.M., 2007. Quantifying hillslope erosion rates and processes for a coastal California landscape over varying timescales. Earth Surf. Process. Landforms 32, 544–560.

Olsen, C.R., et al., 1985. Atmospheric fluxes and marsh-soil inventories of Be-7 and Pb-210. J. Geophys. Res. Atmos. 90 (ND6), 487–495.

Paton, T.R., Humphries, G.S., Mitchell, P.B., 1995. Soils: A New Global View. UCL Press Limited, London, p. 213.

Pelletier, J.D., Rasmussen, C., 2009. Quantifying the climatic and tectonic controls on hillslope steepness and erosion rate. Lithosphere 1, 73–80.

Porto, P., Walling, D.E., Tamburino, V., Callegari, G., 2003. Relating caesium-137 and soil loss from cultivated land. Catena 53 (4), 303–326.

Prosser, I.P., Dietrich, W.E., 1995. Field experiments on erosion by overland flow and their implication for a digital terrain model of channel initiation. Water Resour. Res. 31, 2867–2876.

Quine, T.A., Govers, G., Walling, D.E., Zhang, X.B., Desmet, P.J.J., Zhang, Y.S., Vandaele, K., 1997. Erosion processes and landform evolution on agricultural land – new perspectives from caesium-137 measurements and topographic-based erosion modelling. Earth Surf. Process. Landforms 22 (9), 799–816.

Reneau, S.L., Dietrich, W.E., 1990. Depositional history of hollows on steep hillslopes, coastal Oregon and Washington. Natl. Geogr. Res. 6 (2), 220–230.

Reneau, S.L., Dietrich, W.E., 1991. Erosion rates in the southern oregon coast range: evidence for an equilibrium between hillslope erosion and sediment yield. Earth Surf. Process. Landforms 16 (4), 307–322.

Author's personal copy

Riebe, C.S., Kirchner, J.W., Finkel, R.C., 2003a. Long-term rates of chemical weathering and physical erosion from cosmogenic nuclides and geochemical mass balance. Geochim. Cosmochim. Acta 67, 4411–4427.

Riebe, C.S., Kirchner, J.W., Finkel, R.C., 2003b. Sharp decrease in long-term chemical weathering rates along an altitudinal transect. Earth Planet. Sci. Lett. 6393, 1–14.

Riebe, C.S., Kirchner, J.W., Finkel, R.C., 2004. Erosional and climatic effects on long-term chemical weathering rates in granitic landscapes spanning diverse climate regimes. Earth Planet. Sci. Lett. 224, 547–562.

Riebe, C.S., Kirchner, J.W., Granger, D.E., Finkel, R.C., 2000. Erosional equilibrium and disequilibrium in the Sierra Nevada, inferred from cosmogenic Al and Be in alluvial sediment. Geology 28, 803–806.

Riebe, C.S., Kirchner, J.W., Granger, D.E., Finkel, R.C., 2001a. Minimal climatic control on erosion rates in the Sierra Nevada, California. Geology 29, 447–450.

Riebe, C.S., Kirchner, J.W., Granger, D.E., Finkel, R.C., 2001b. Strong tectonic and weak climatic control of long-term chemical weathering rates. Geology 29, 511–514.

Roels, J.M., 1985. Estimation of soil loss at a regional scale based on plot measurements – some critical considerations. Earth Surf. Process. 10, 587–595.

Roering, J.J., Almond, P., Tonkin, P., McKean, J., 2002. Soil transport driven by biological processes over millenial time scales. Geology 30 (12), 1115–1118.

Roering, J.J., Gerber, M., 2005. Fire and the evolution of steep, soil-mantled landscapes. Geology 33, 349–352.

Roering, J.J., Kirchner, J.W., Dietrich, W.E., 1999. Evidence for non-linear, diffusive sediment transport on hillslopes and implications for landscape morphology. Water Resour. Res. 35 (3), 853–870.

Roering, J.J., Kirchner, J.W., Sklar, L.S., Dietrich, W.E., 2001. Hillslope evolution by nonlinear creep and landsliding: an experimental study. Geology 29, 143–146.

Rosenbloom, N.A., Anderson, R.S., 1994. Hillslope and channel evolution in a marine terraced landscape, Santa Cruz, California. J. Geophys. Res. 99 (B7), 14,013–14,029.

Schaetzl, R.J., Follmer, L.R., 1990. Longevity of treethrow microtopography: implications for mass wasting. Geomorphology 3, 113–123.

Schoeneberger, P.J., Amoozegar, A., Buol, S.W., 1995. Physical property variation of a soil and saprolite continuum at 3 geomorphic positions. Soil Sci. Soc. Am. J. 59 (5), 1389–1397.

Selby, M.J., 1980. A rock mass strength classification for geomorphic purposes: with tests from Antarctica and New Zealand. Zeitschrift fur Geomorphologie N. F. 24 (1), 31–51.

Selby, M.J., 1985. Hillslope Materials and Processes. Oxford University Press, Oxford, England.

Simon, S.L., Bouville, A., Beck, H.L., 2004. The geographic distribution of radionuclide deposition across the continental US from atmospheric nuclear testing. J. Environ. Radioact. 74 (1–3), 91–105.

Steegen, A., Govers, G., Takken, I., Nachtergaele, J., Poesen, J., Merckx, R., 2001. Factors controlling sediment and phosphorus export from two Belgian agricultural catchments. J. Environ. Qual. 30 (4), 1249–1258.

Tyler, A.N., Carter, S., Davidson, D.A., Long, D.J., Tipping, R., 2001. The extent and significance of bioturbation on Cs-137 distributions in upland soils. Catena 43 (2), 81–99.

U.S. ERDA (United States Energy Research and Development Administration), 1977, Final Tabulation of Monthly 90Sr Fallout Data: 1954–1976: New York, Environmental Measurements Laboratory, Report HASL-329.

Viles, H., A., Goudie, A., Grab, S., Lalley, J., 2011. The use of the schmidt hammer and equotip for rock hardness assessment in geomorphology and heritage science: a comparative analysis. Earth Surf. Process. Landforms 36, 320–333.

Author's personal copy

Wallbrink, P.J., Murray, A.S., 1996. Distribution and variability of Be-7 in soils under different surface cover conditions and its potential for describing soil redistribution processes. Water Resour. Res. 32 (2), 467–476.

Walling, D.E., He, Q., 1999. Using fallout lead-210 measurements to estimate soil erosion on cultivated land. Soil Sci. Soc. Am. J. 63 (5), 1404–1412.

Walling, D.E., He, Q., Blake, W., 1999. Use of Be-7 and Cs-137 measurements to document short- and medium-term rates of water-induced soil erosion on agricultural land. Water Resour. Res. 35 (12), 3865–3874.

Walling, D.E., Russell, M.A., Hodgkinson, R.A., Zhang, Y., 2002. Establishing sediment budgets for two small lowland agricultural catchments in the UK. Catena 47 (4), 323–353.

West, A., Galy, A., Bickle, M., 2005. Tectonic and climatic controls on silicate weathering. Earth and Planetary Science Letters 235 (1–2), 211–228.

White, A.F., Brantley, S.L., 2003. The effect of time on the weathering of silicate minerals: why do weathering rates differ in the laboratory and field? Chem. Geol. 202 (3–4), 479–506.

White, A.F., Blum, A.E., Schulz, M.S., Bullen, T.D., Harden, J.W., Peterson, M.L., 1996. Chemical weathering rates of a soil chronosequence on granitic alluvium. 1. Quantification of mineralogical and surface area changes and calculation of primary silicate reaction rates. Geochim. Cosmochim. Acta 60 (14), 2533–2550.

Whiting, P.J., Bonniwell, E.C., Matisoff, G., 2001. Depth and areal extent of sheet and rill erosion based on radionuclides in soils and suspended sediment. Geology 29, 1131–1134.

Wilson, C.G., Matisoff, G., Whiting, P.J., 2003. Short-term erosion rates from a Be-7 inventory balance. Earth Surf. Process. Landforms 28 (9), 967–977.

Yoo, K., Amundson, R., Heimsath, A.M., Dietrich, W.E., Brimhall, G.H., 2007. Integration of geochemical mass balance with sediment transport to calculate rates of soil chemical weathering and transport on hillslopes. J. Geophys. Res. Earth Surf. 112 (F2).

Young, A., 1960. Soil movement by denudational processes on slopes. Nature 188, 120–122.

Young, A., 1963. Some field observations of slope form and regolith, and their relation to slope development. Trans. Inst. Br. Geogr. 32, 1–29.

Zhang, X.B., Quine, T.A., Walling, D.E., Li, Z., 1994. Application of the cesium-137 technique in a study of soil-erosion on gully slopes in a yuan area of the loess plateau near Xifeng, Gansu Province, China. Geogr. Ann. Phys. Geogr. 76 (1–2), 103–120.

Zimbone, S.M., Vickers, A., Morgan, R.P.C., Vella, P., 1996. Field investigations of different techniques for measuring surface soil shear strength. Soil Technol. 9 (1–2), 101–111.